JOURNAL OF GEOPHYSICAL RESEARCH, VOL. 111, D22210, doi:10.1029/2005JD006707, 2006

Evaluation of aerosol distribution and optical depth in the Geophysical Fluid Dynamics Laboratory coupled model CM2.1 for present climate

Paul Ginoux,[1] Larry W. Horowitz,[1] V. Ramaswamy,[1] Igor V. Geogdzhayev,[2] Brent N. Holben,[3] Georgiy Stenchikov,[4] and Xuexi Tie[5]

Received 25 September 2005; revised 5 May 2006; accepted 16 June 2006; published 21 November 2006.

[1] This study evaluates the strengths and weaknesses of aerosol distributions and optical depths that are used to force the GFDL coupled climate model CM2.1. The concentrations of sulfate, organic carbon, black carbon, and dust are simulated using the MOZART model (Horowitz, 2006), while sea-salt concentrations are obtained from a previous study by Haywood et al. (1999). These aerosol distributions and precalculated relative-humidity-dependent specific extinction are utilized in the CM2.1 radiative scheme to calculate the aerosol optical depth. Our evaluation of the mean values (1996–2000) of simulated aerosols is based on comparisons with long-term mean climatological data from ground-based and remote sensing observations as well as previous modeling studies. Overall, the predicted concentrations of aerosol are within a factor 2 of the observed values and have a tendency to be overestimated. Comparison with satellite data shows an agreement within 10% of global mean optical depth. This agreement masks regional differences of opposite signs in the optical depth. Essentially, the excessive optical depth from sulfate aerosols compensates for the underestimated contribution from organic and sea-salt aerosols. The largest discrepancies are over the northeastern United States (predicted optical depths are too high) and over biomass burning regions and southern oceans (predicted optical depths are too low). This analysis indicates that the aerosol properties are very sensitive to humidity, and major improvements could be achieved by properly taking into account their hygroscopic growth together with corresponding modifications of their optical properties.

Citation: Ginoux, P., L. W. Horowitz, V. Ramaswamy, I. V. Geogdzhayev, B. N. Holben, G. Stenchikov, and X. Tie (2006), Evaluation of aerosol distribution and optical depth in the Geophysical Fluid Dynamics Laboratory coupled model CM2.1 for present climate, *J. Geophys. Res.*, *111*, D22210, doi:10.1029/2005JD006707.

1. Introduction

[2] Aerosols scatter and absorb short-wave and long-wave radiation, thereby perturbing the energy budget of the Earth-atmosphere system. Such effects from anthropogenic aerosols exert a direct radiative forcing of climate, but its quantification is difficult due to the large spatial and temporal variability of both the composition and distribution of aerosol [*Ramaswamy et al.*, 2001]. In that regard, the global coverage of atmospheric in situ measurements is still not sufficient for a proper evaluation of the role of aerosols on climate. Consequently, climate and aerosol models have been the primary instruments utilized for the Third Assessment Report (TAR) of the Intergovernmental Panel on Climate Change (IPCC) to assess aerosol forcing [*Penner et al.*, 2001]. The wide range of results from different aerosol models indicates that significant uncertainties remain, particularly concerning the role of organic and black carbon aerosols [*Penner et al.*, 2001].

[3] Because of computer limitations, most coupled climate models cannot afford to solve prognostic equations for aerosol concentrations. Instead, their distributions are simulated off-line with chemical transport models (CTMs), which are driven by meteorological fields either from reanalysis (for simulation of the last few decades) or GCM (for past and future simulations). Climatological monthly mean distributions calculated from the CTM simulation are then used as an input for the radiative scheme of the coupled climate models. Since the IPCC TAR, the characterization of aerosols on regional and global scales has been improved considerably with developments that include new parameterizations in CTM, new satellite instruments, longer data records of monitoring stations, and

[1]NOAA Geophysical Fluid Dynamics Laboratory, Princeton, New Jersey, USA.
[2]Department of Applied Physics and Applied Mathematics, Columbia University and NASA Goddard Institute for Space Studies, New York, New York, USA.
[3]NASA Goddard Space Flight Center, Greenbelt, Maryland, USA.
[4]Department of Environmental Sciences, Rutgers–The State University of New Jersey, New Brunswick, New Jersey, USA.
[5]National Center for Atmospheric Research, Boulder, Colorado, USA.

0148-0227/06/2005JD006707$09.00

recent field campaigns. Such recent improvements now allow models to simulate multiple species of aerosol, as well as their sources, optical properties, and hygroscopic growth. Evaluation of these latest developments with available data sets constitutes a crucial part of any assessment.

[4] In the framework of the 2007 IPCC Fourth Assessment Report (AR4), aerosol distributions have been simulated over the period 1860–2100 with the MOZART 2 (Model for Ozone and Related chemical Tracers, version 2) chemical transport model [*Horowitz et al.*, 2003]. These aerosol distributions are part of the set of historical, present and future short-lived forcing agents in the Geophysical Fluid Dynamics Laboratory (GFDL) coupled climate model CM2.1 simulations for AR4 [*Delworth et al.*, 2006]. Among these agents, the tropospheric aerosols include: sulfate ($SO_4^=$), black carbon (BC), organic carbon (OC), mineral dust and sea salt. The present paper aims to evaluate the "present-day" (1996–2000) mean aerosol distributions and optical depths used in CM2.1. From the historical run (1860–2000), we select the period 1996–2000 as representative of the present climate for two reasons. First, as shown in section 4.2.1, the influence of volcanic aerosols on AOD is negligible after 1996. Second, the CM2.1 simulations after 2000 use different IPCC scenarios, and any analysis of the results as a function of the scenarios is beyond the scope of this article. The evaluation is based on comparisons with climatological values of ground-based and remote sensing observations, as well as with results from other aerosol modeling studies. In nearly all cases, the data sets cover several years of records and their mean values are considered as climatological observations.

[5] After providing a brief description of the models and the aerosol fields in section 2 and 3, respectively, we first compare the annual mean values of surface concentration and aerosol optical depth with individual data sets in section 4. Then, in section 5 we combine the data sets to compare simultaneously the seasonal variation of surface concentration and AOD for various environments. In our conclusions, given in section 6, we highlight the strengths and weaknesses of the model results and provide suggestions for improvements.

[6] This paper is the second in a series of three. In the first one, *Horowitz* [2006] describes the MOZART simulations of ozone and aerosol distribution, evaluates the ozone concentrations, and describes the sensitivity of model results to wet removal rates for aerosols. The third paper (in preparation) presents and evaluates the instantaneous radiative forcing resulting from natural and anthropogenic agents, including the short-lived ones (aerosols and ozone).

2. Model Description

2.1. Coupled Model CM2.1 and MOZART

[7] The CM2.1 coupled climate model is designed to simulate past, present and future climates. A description of the model and of the simulation performed for the AR4 are provided by *Delworth et al.* [2006]. Here details of the atmospheric model and the implementation of the aerosol radiative forcing are briefly described. The atmospheric model (AM2) has a horizontal resolution of 2° latitude by 2.5° longitude, and 24 vertical levels. The dynamical core is based on the finite volume technique developed by *Lin* [2004]. The atmospheric physical parameterizations are described in detail by the *GFDL Global Atmospheric Model Development Team* [2004], including the treatment of scattering and absorption of radiation by aerosols. As CM2.1 does not calculate aerosol distributions, three-dimensional (3-D) monthly mean fields of mass concentration and optical properties of aerosols are provided to the radiative scheme. The prescribed aerosols include sulfate, black carbon, organic carbon, dust, and sea salt. Sea-salt monthly concentrations are obtained from a previous study by *Haywood et al.* [1999]. They have assumed a surface concentration proportional to the wind speed using the parameterization by *Lovett* [1978]. Sea salt vertical concentration is assumed constant from the surface to 850 hPa, and zero above, and this distribution is kept constant over the years during the simulations.

[8] All aerosol distributions, except for sea salt, have been simulated with MOZART 2, a global 3D chemical transport model. MOZART has been described in detail by *Horowitz et al.* [2003] for the gas phase chemistry and *Tie et al.* [2005] for the implementation of aerosols. *Horowitz* [2006] describes the particular simulations of past, present and future concentrations of aerosol and gas species used within CM2.1 for AR4. The MOZART simulations of gaseous species and aerosol distributions, except for dust, were driven by meteorological fields computed by the NCAR Community Climate Model (MACCM3) [*Kiehl et al.*, 1998]. The horizontal resolution of MOZART driven by MACCM3 is 2.8° by 2.8° which is comparable to that of AM2. Dust distribution is simulated for 1992–1994 by using NCEP/NCAR reanalysis fields and a 1.9° by 1.9° horizontal resolution. The dust sources are from *Ginoux et al.* [2001]. Decadal records of monthly aerosol concentration for 1860–2100 are produced by running MOZART for two years every decade with varying emissions but the same climatological "present-day" MACCM3 meteorological fields (see *Horowitz* [2006] for details). The monthly mean 3D concentrations from the second year are then remapped to the 2 by 2.5 degrees CM2.1 grid and applied in the climate simulations. The year to year variations are imposed by linear interpolation between decadal monthly concentrations, except for dust which is held constant. As emissions of dust and sea salt are assumed to be natural, they do not contribute to the radiative forcing.

2.2. Aerosol Optical Depth

[9] During the CM2.1 simulation, at every radiative time step (3 hours), the aerosol optical depth, single scattering albedo, and asymmetry parameter are calculated by considering hygroscopic growth. This calculation is performed by using the aerosol concentration interpolated from MOZART, the optical properties of a single particle derived from Mie calculations, and the relative humidity simulated at the current time step.

[10] Aerosol optical depth (AOD) is calculated from the dry mass concentration, the specific extinction coefficients (α_e), and the relative humidity (RH). The specific extinction coefficients are calculated from Mie theory on the basis of size distributions, refractive indices, particle density, and hygroscopic properties. These properties have been described in detail by *Haywood and Ramaswamy* [1998] for sulfate and black carbon. Here we briefly summarize the

Table 1. Physical and Optical Properties of Aerosols at 550 nm[a]

Aerosol Type	r_e, μm	ρ_0, kg m^{-3}	α_e (dry), m^2 g^{-1}	α_e (80% RH), m^2 g^{-1}	α_e (100% RH), m^2 g^{-1}
$(NH_4)_2SO_4$	0.166	1769	3.62	9.7	130
BC	0.039	1000	9.26	-	-
OC	0.087	1800	3	-	-
Salt	-	2160	-	2.5	-
Dust	0.1	2650	1.71	-	-
Dust	0.2	2650	3.22	-	-
Dust	0.4	2650	2.42	-	-
Dust	0.8	2650	0.97	-	-
Dust	1	2500	0.74	-	-
Dust	2	2500	0.34	-	-
Dust	4	2500	0.16	-	-
Dust	8	2500	0.08	-	-

[a]Here ρ_0 is the dry aerosol density, r_e is the effective mass radius, and α_e is the specific extinction coefficient at 550 nm and given relative humidity (RH).

most relevant properties. Sulfate aerosols are considered optically as ammonium sulfate using values for the refractive index from the work by *Toon et al.* [1976]. Black carbon is modeled with a value for the refractive index from the *World Climate Program* (*WCP*) [1986]. As proposed by *WCP* [1986], dust is treated as if it were all Saharan, with a refractive index based on the work by *Patterson et al.* [1977] in the ultraviolet and visible and by *Volz* [1973] for longer wavelengths. Recent studies based on Sun photometry data [*Dubovik et al.*, 2002] and satellite data in the near ultraviolet [*Sinyuk et al.*, 2003] and visible [*Kaufman et al.*, 2001] regions show that dust in the atmosphere is much less absorbing than the samples of Sahara dust collected by *Patterson et al.* [1977]. MOZART provides bulk mass concentration for sulfate, OC and BC. Following the work by *Haywood and Ramaswamy* [1998], a lognormal size distribution is assumed for the number of sulfate and black carbon particles with a fixed geometric mean radius (0.05 μm for sulfate and 0.0118 μm for black carbon) and standard deviation (2 for sulfate and black carbon). For dust, the mass size distribution in MOZART is discretized from 0.1 to 10 μm into 8 bins. Optical properties for each size bin are based on the study by *Tegen and Lacis* [1996].

[11] For sea salt, the values of mass extinction coefficients for the accumulation and coarse modes are given by *Haywood et al.* [1999]. The mass extinction coefficient for organic carbon is half the value reported by *Haywood et al.* [1999], and correspond to the values attributed for organic matter, but owing to coding error the organic concentrations have not been converted to organic matter before performing the radiative calculation in CM2.1. The total AOD is obtained by adding together the contributions from the various aerosol species, assuming that they are externally mixed.

[12] The effect of hygroscopic growth on the extinction coefficients is considered for sulfate and sea salt. Sea salt is assumed to be in a maritime environment with a constant relative humidity of 80%, while sulfate extinction varies with the calculated relative humidity from CM2.1 at every time step and grid point. As indicated in Table 1, the extinction coefficient of sulfate increases by more than a factor of 10 as the relative humidity increases from 80% to 100%. The hygroscopic growth of sulfate between 30% and 80% RH is obtained using the method of *Haywood and Ramaswamy*, [1998], and between 81% RH and 100% from the approximation formula by *Fitzgerald* [1975]. The sulfate extinction is calculated in CM2.1 by linearly interpolating between precalculated extinctions archived for specific RH values in a "look-up" table with a step of 2% between 80 and 98% and then a step of 1%. The density of wet particles is the volume-weighted density of dry aerosol and water. Organic carbon, black carbon and dust particles are assumed to be hydrophobic, and their properties are independent of relative humidity.

2.3. Volcanic Aerosols

[13] The objective of this manuscript is not to evaluate the accuracy of the simulation of volcanic aerosols; rather, it is to include their contribution in the time series of AOD, as they significantly impact the total AOD after major eruptions. All major explosive volcanic eruptions are included as forcing in CM2.1, as well as smaller ones that produced detectable perturbations of stratsopheric optical depth (see *Stenchikov et al.* [2006] for details). The calculation of spectral optical characteristics of volcanic aerosols for the GFDL CM2.1 models was based on visible aerosol extinctions and effective radii compiled by *Sato et al.* [1993] and *Hansen et al.* [2002]. A lognormal aerosol size distribution was assumed. The aerosol effective radii of *Hansen et al.* [2002] were modified using Upper Atmosphere Research Satellite (UARS) observations for the Pinatubo period, accounting for their variations with altitude, especially at the top of the aerosol layer above 10–20 hPa where particles are very small. Then, aerosol optical characteristics were calculated with the Mie algorithm following *Stenchikov et al.* [1998] and *Ramachandran et al.* [2000]. The volcanic impacts in the IPCC AR4 models, including CM2.1, are analyzed by *Stenchikov et al.* [2006].

3. Model Results

3.1. Zonal Profiles

[14] Figure 1 shows the zonal annual mean (1996–2000) concentrations for sulfate, organic carbon, black carbon, and dust and sea-salt aerosols. Sulfate and carbonaceous aerosols have maxima at the surface in northern midlatitudes. Carbonaceous aerosols display a secondary maximum in the tropical regions, associated with biomass burning. Dust has its maximum near the surface in the northern subtropics, and is the most abundant aerosol throughout the atmosphere, except in the southern high latitudes. At these latitudes, sulfate and sea salt are the dominant species above and in the boundary layer, respectively. The pattern of zonal mean profiles for carbonaceous aerosols shown here differs considerably from that of *Reddy and Boucher* [2004]. While the surface concentrations in the two studies are similar, the location of maxima and vertical mixing in the boundary layer are significantly different. These differences can be attributed to the treatment of aerosol emissions. First, they use fire counts from satellite to constrain the spatial, seasonal and interannual variations of emission by biomass burning. Second, they distribute the emitted aerosols from biomass burning vertically throughout the boundary layer, while all emission fluxes are placed in the surface layer of our model. The proper way to evaluate both distributions would be to compare with observed aerosol concentration profiles, which unfortunately are scarce.

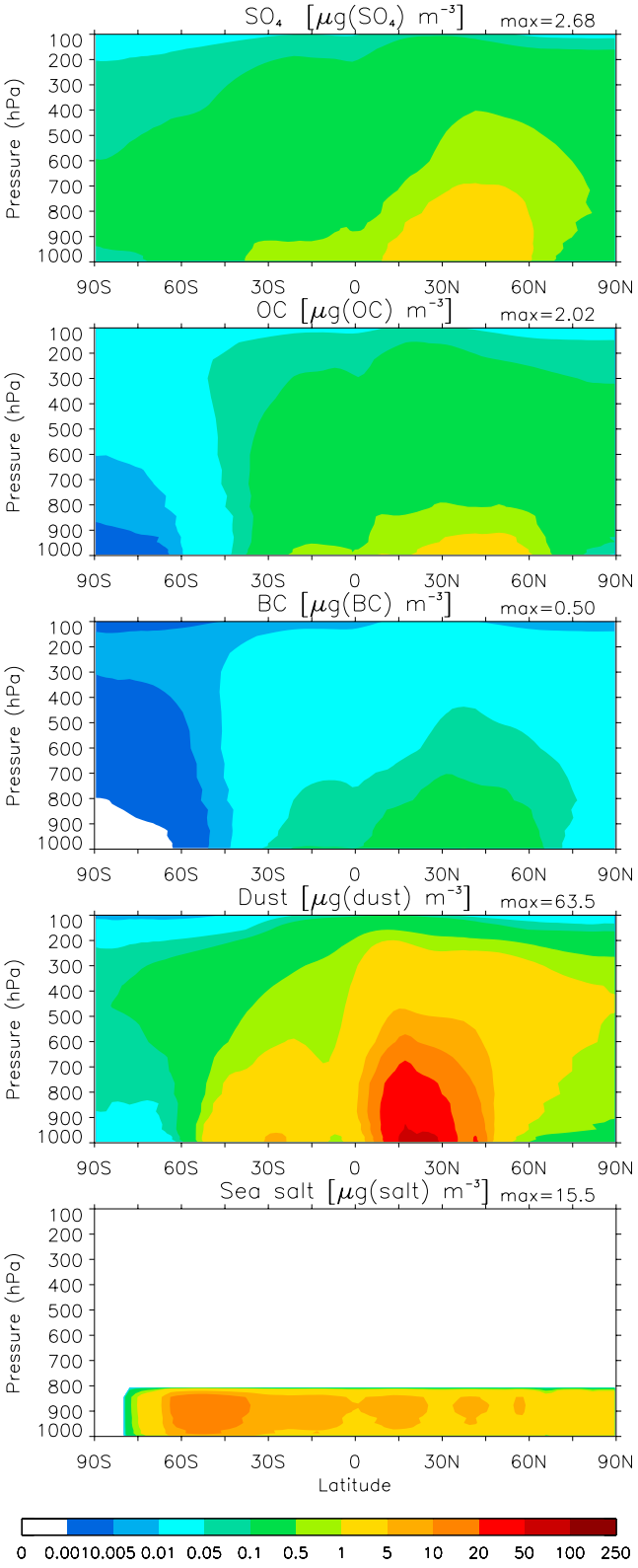

Figure 1. Model-simulated zonal annual mean (1996–2000) sulfate, black carbon, organic carbon, dust, and sea-salt concentrations (μg m^{-3}) from the surface to 100 hPa.

3.2. Global Distribution

[15] Figure 2 shows the annual mean (1996–2000) distributions of column burdens, optical depth (at 550 nm) and percentage contributions to the total optical depth of $SO_4^=$, OC, BC, sea salt, and dust. Only $SO_4^=$ has a nonlinear relationship between column burden and AOD, as it depends on relative humidity. The larger ratio between AOD and column burden for $SO_4^=$ at high latitudes is associated with the high relative humidity at these latitudes. This reveals the higher sensitivity of AOD to the sulfate loading over the industrialized countries in the Northern Hemisphere. Carbonaceous aerosols are largest over eastern Asia and eastern Europe, while biomass burning regions are seen in South America, Africa, and South Asia. Peak values for dust are located over or downwind of the arid regions. The long-range transport over the oceans is clearly visible for each aerosol, except for sea salt which is not transported in the model. The contribution of sulfate to the AOD dominates globally (56%) over sea salt (20%), dust (13%), OC (7%) and BC (4%), and also regionally, except over northern Africa where dust dominates by more than 50%. Over most oceans, the contribution from sulfate dominates, followed by that from sea salt.

3.3. Comparison With Other Models

[16] Table 2 compares the total mass loading of each aerosol type used in CM2.1 with studies by *Chin et al.* [2002], *Tie et al.* [2005], and *Reddy et al.* [2005]. Table 3 gives the values of global mean AOD for the same studies. The CM2.1 mass loadings are within 30% of other studies, except for sea salt which is a factor 2 to 5 lower.

[17] In Table 3, we notice that the spread between CM2.1 and other models is more than a factor 2 for sulfate, but less than 15% for sea salt. This spread is very different from that in Table 2, and this difference is due to values of mass extinction coefficients. This shows that when comparing optical depth, the optical properties and in the case of hygroscopic particles, the relative humidity is as important as the aerosol concentration. As the extinction properties for dry particles given in Table 1 are similar to those in other studies, it would seem that the difference lies in the treatment of hygroscopic growth. An exception is for the specific extinction of dry organic aerosols (see Table 1) which is a factor 2 lower than previous studies. In addition, other models include the hygroscopic growth of OC in the calculation of specific extinction. Thus the difference in optical depth of organic aerosols can be a factor 3 or more higher. *Ming et al.* [2005] have shown that the inclusion of water uptake by organic aerosols increases the specific extinction coefficient by more than a factor of 3 at 95% relative humidity. Another source of discrepancy with other model studies is the use of a cutoff to distinguish haze particles and cloud droplets. In our case, sulfate aerosols are allowed to grow up to 100% RH, while most other modeling studies use a cutoff of 99% relative humidity and some imposed even lower limits (e.g., 95% in the work of *Reddy et al.* [2005]). There is at least one in situ measurement of marine aerosol growing up to 98.5% by *Wulfmeyer and Feingold* [2000]. In our aerosol model, the specific extinction of ammonium-sulfate increases from 71 m^2 g^{-1} at 99% to 130 m^2 g^{-1} at 100% RH. As there are no laboratory measurements of growth and optical properties beyond

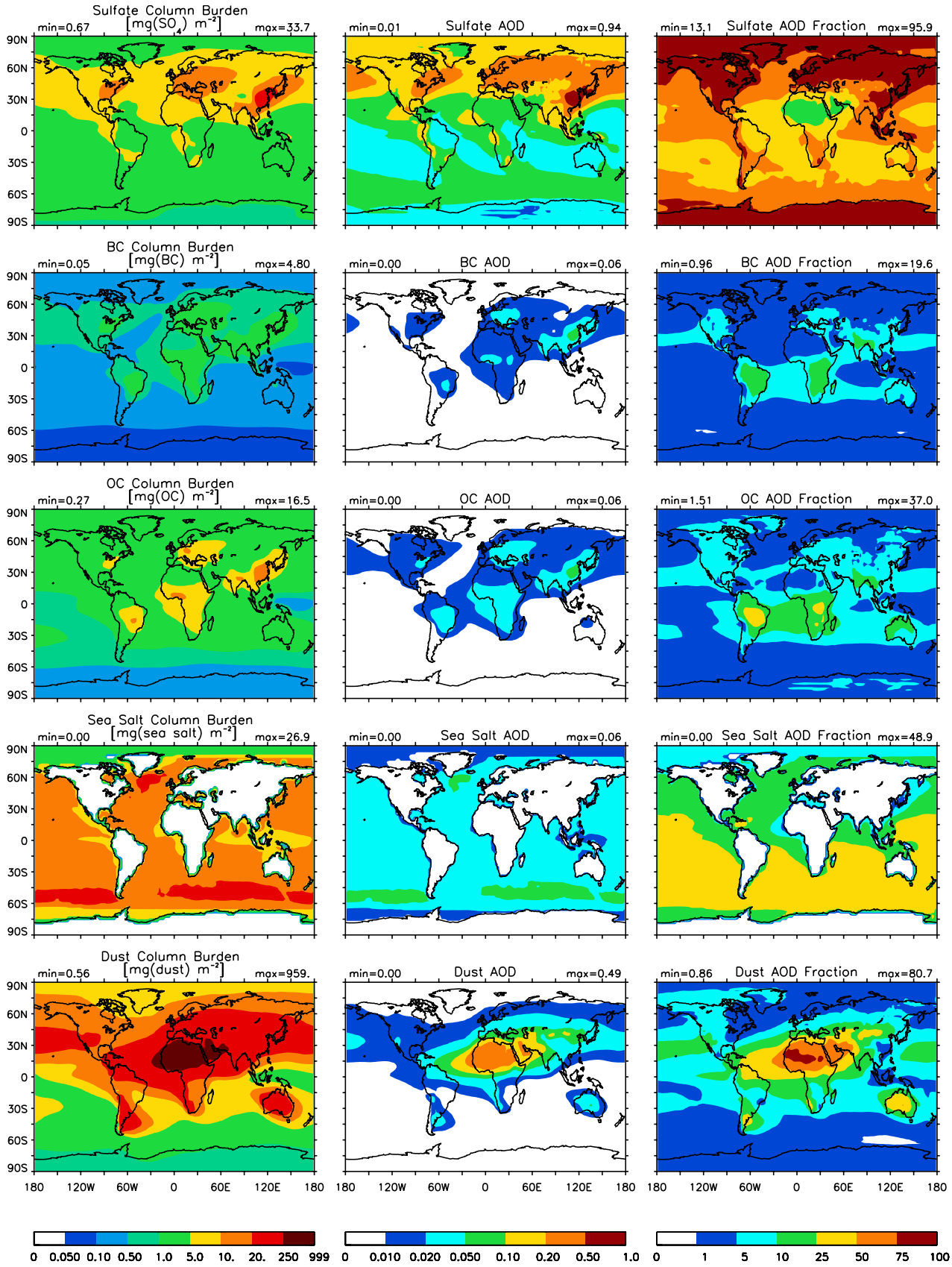

Figure 2. Model-simulated annual mean (1996–2000) (left) distribution of sulfate, organic carbon, black carbon, dust, and sea-salt burdens (mg m^{-2}), (middle) tropospheric aerosol optical depth at 550 nm (dimensionless), and (right) fractional contribution to the optical depth of tropospheric aerosols (%). The minimum and maximum values plotted in each panel are indicated on the top left and right, respectively.

Table 2. Total Mass Loading of Each Aerosol Component[a]

	This Study	*Chin et al.* [2002]	*Reddy et al.* [2005]	*Tie et al.* [2005]
SO_4	2.5	1.9	2.2	2.2
BC	0.3	0.3	0.4	0.45
OC	1.4	1.4	1.2[b]	2
Salt	5	11	9	26
Dust	22.5	29	23	30

[a]Units are Tg.
[b]After dividing by 1.5 to convert organic matter (OM) to OC.

98% RH, the values have been extrapolated. It is possible that the extrapolated values are largely overestimated.

[18] Another possibility is that the frequency of RH values greater than 99% is too high. *Myhre et al.* [2004a] have analyzed different data sets of RH including the one simulated by the GFDL "Manabe Climate Model" described by *Delworth et al.* [2002]. They found that about 8% of the model grid points have a relative humidity higher than 95%, which is twice the number of corresponding points in the European Centre for Medium-Range Weather Forecasts (ECMWF) data set. However, the study by *Myhre et al.* [2004a] does not reflect the extensive new developments within the GFDL Atmospheric model [*GFDL Global Atmospheric Model Development Team*, 2004] and included in CM2.1 coupled climate model.

[19] A comprehensive analysis on the handling of hygroscopic optical properties of sulfate aerosols in the presence of high RH is needed to improve this large source of uncertainty.

4. Comparison With Individual Data Sets

4.1. Surface Concentration

[20] In this section we compare the present climatology (1996–2000) of aerosol concentrations at the surface with three data sets from the University of Miami, the Interagency Monitoring of Protected Visual Environments (IMPROVE) program, and the European Monitoring and Evaluation Program (EMEP).

4.1.1. University of Miami Data Set

[21] The mass concentration of sulfate, dust, and sea salt have been collected continuously by the University of Miami at 28 stations, mostly on islands, over the past 2 or even 4 (in the case of the Barbados station) decades [*Savoie and Prospero*, 1989; *Prospero*, 1996]. The data set has commonly been used for the evaluation and intercomparison of models [e.g., *Penner et al.*, 2001]). The monthly mean values and their standard deviation for the entire records are used in our comparisons. Figure 3 shows the comparison of annual mean sulfate, dust, and sea-salt concentrations at the surface in CM2.1 and as observed. The correlation coefficients between observed and simulated values for sulfate and dust are 0.95 and 0.97, respectively. The concentrations are spread over more than 3 orders of magnitude. The sea-salt observations show similar variability in observed concentrations, but the model values vary by less than 1 order of magnitude and are several order of magnitude lower than observed at most sites. Also in Figure 3, the global distribution of simulated annual mean concentration is shown in addition to the ratio between the simulated and observed concentration at each site. The simulated sulfate concentrations are within a factor of 2 of the observations at 80% of the stations, with some exceptions in the southern oceans and Bermuda, where sulfate is overestimated and underestimated respectively by up to a factor 3. *Horowitz* [2006] evaluated the sensitivity of aerosol concentrations to wet removal rates. He shows that doubling the removal rate decreases the sulfate concentration over remote ocean regions by 60%. However, increasing the rate of wet removal will further increase the discrepancy in other stations like Bermuda. Regarding dust concentrations, large differences arise in remote regions, in particular over Antarctica where dust is underestimated by more than a factor of 5. *Genthon* [1992] has shown the difficulty in reproducing observed dust concentrations at the surface of Antarctica, as a strong inversion layer decouples the surface from the free troposphere in which dust is transported from distant sources.

4.1.2. IMPROVE Data Set

[22] The Interagency Monitoring of Protected Visual Environments (IMPROVE) program [*Malm et al.*, 1994] has collected aerosol samples twice weekly starting from 1988 at almost 200 sites located in National Parks of the United States. The concentration of $SO_4^=$, OC, BC, and submicron dust particles are measured from PM2.5 samples. Their climatological monthly values have been calculated by averaging valid data over the entire records. Taking advantage of the relative homogeneity of the spatial distribution of the IMPROVE sites, the data have been interpolated onto a 1 degree grid over the United States. The interpolation weights the data inversely with the square of its distance to the grid point. The values of CM2.1 on the 2 by 2.5 degrees grid are then compared with the closest 1 by 1 grid point of IMPROVE data. Figure 4 shows the gridded IMPROVE data over the United Sates, the CM2.1 results, and the relative difference between the two. For each aerosol type, CM2.1 reproduces correctly the location of maxima and minima. Sulfate and carbonaceous aerosols are typically simulated to within a factor of 2, but tend to be overestimated. Sulfate concentrations are overestimated by about 50% in the polluted Northeast, but are up to a factor of 5 too high compared to background concentrations in the Northwest. For organic aerosols, the simulated values are generally within a factor of 2 of the measurements. The largest discrepancy for black carbon is over New England where the peak concentration is overestimated by up to a factor of 5. However, this is likely to be a resolution issue rather than a modeling problem. In Alaska and some parts of the northwestern United States, carbonaceous aerosols are underestimated by up to a factor of 2. A similar discrepancy has been reported in other studies [e.g., *Liousse et al.*, 1996; *Chung and Seinfeld*, 2002; *Reddy and Boucher*, 2004], and has been attributed to a lack of proper modeling of boreal forest fires. In all other states, most studies obtain concen-

Table 3. Global Annual Average Aerosol Optical Depth for Each Aerosol Component

	This Study	*Chin et al.* [2002]	*Reddy et al.* [2005]	*Tie et al.* [2005]
SO_4	0.1	0.04	0.04	0.04
BC	0.008	0.007	0.004	0.01
OC	0.011	0.017	0.021	0.036
Salt	0.023	0.027	0.027	0.028
Dust	0.03	0.05	0.026	0.027

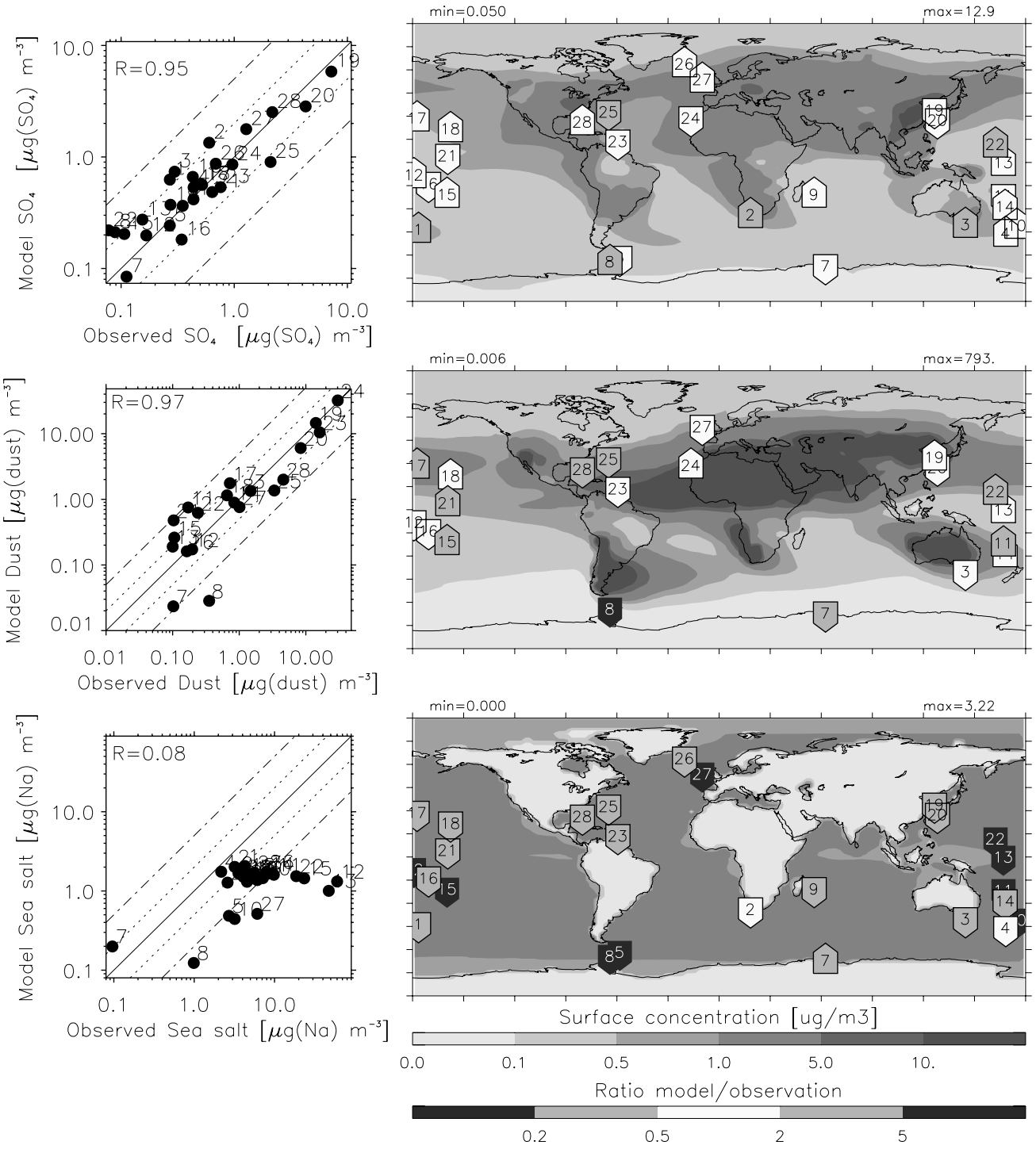

Figure 3. Comparison of simulated (CM2.1, 1996–2000 average) and observed (University of Miami) annual mean surface concentration (μg m^{-3}) of (top) sulfate, (middle) dust, and (bottom) sea-salt sodium at (left) 28 locations and (right) their ratio (simulated by observed) at each location. The ratios are represented with polygons pointing up or down as its value is greater or less than 1. The polygons are white, gray, or black, corresponding to simulated values within a factor 2, 5, or 10 of the observations, respectively. The factor 2 and 5 deviations between CM2.1 and the observations are shown on Figure 3 (left) with dotted and dashed lines, respectively. The correlation coefficients are indicated on the top left in Figure 3 (left). The minimum and maximum simulated concentrations (μg m^{-3}) are indicated above the plots for each aerosol component in Figure 3 (right).

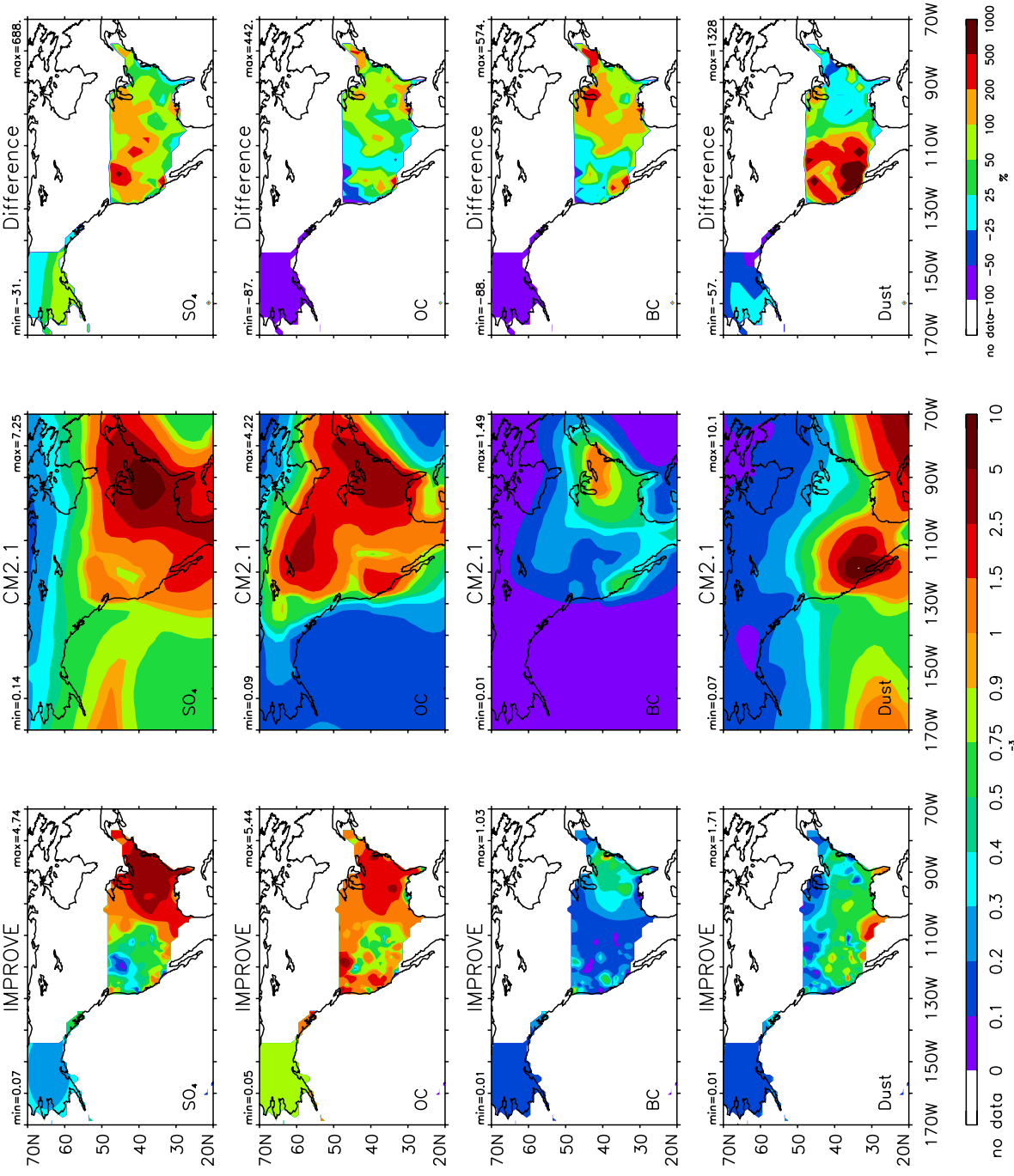

Figure 4. Comparison of (left) IMPROVE PM2.5 and (middle) CM2.1 surface concentrations (μg m^{-3}) and (right) their relative difference in percentage for sulfate (first row), organic carbon (second row), black carbon (third row), and fine dust (fourth row) over North America.

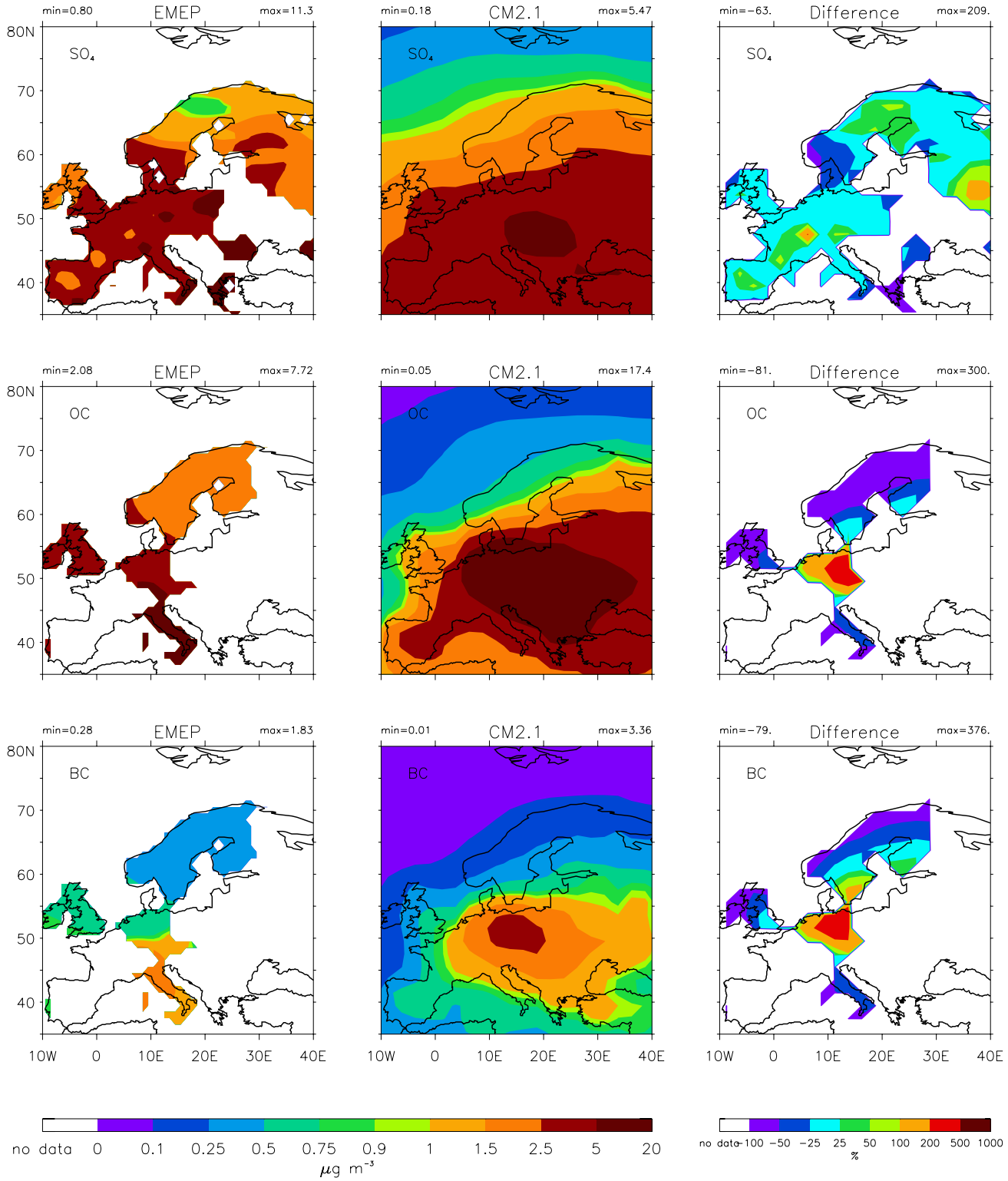

Figure 5. Comparison of (left) EMEP PM10 and (middle) CM2.1 surface concentrations (μg m^{-3}) and (right) their relative difference in percentage for sulfate (first row), organic carbon (second row), and black carbon (third row) over Europe.

trations that are lower than observed for carbonaceous aerosols, in contrast with this work. An exception is the work by *Takemura et al.* [2000] who also overestimated organic carbon concentrations at most IMPROVE stations. This difference between models can be explained by the difficulty of constraining fossil fuel emission of carbonaceous aerosols. Submicron dust concentrations are overestimated by more than a factor of 5 in the Southwest. As the dust sources over the United States are located in that region, the origin of such a large discrepancy is most likely coming from the parameter-

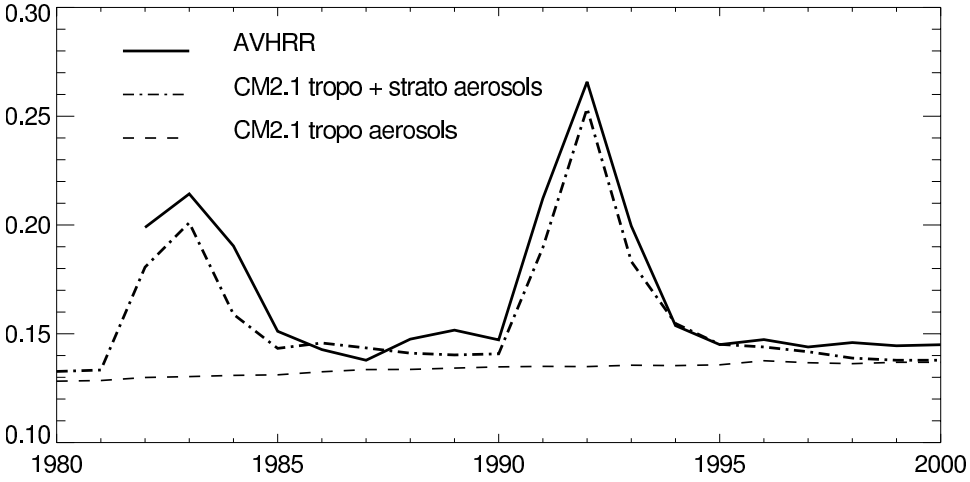

Figure 6. Time series of the global oceanic annual mean aerosol optical depth at 550 nm retrieved from AVHRR (solid line, from 1982 to 2000), simulated (CM2.1) with tropospheric aerosols (dashed line, from 1980 to 2000), and both tropospheric and volcanic aerosols (dash-dotted line, from 1980 to 2000).

ization of emissions, such as an overestimation of the soil fraction of submicron particles, the surface winds or source area. IMPROVE dust concentration are not directly measured, but rather are estimated from the abundance of some measured elements. The fraction of each element is assumed to be constant in the chemical composition of dust (see *Malm et al.* [1994] for details). *Goudie and Middleton* [2001] reviewed the chemical composition of samples collected from deserts of various continents, and showed significant variability for some chemical elements. In the case of intercontinental transport of dust to the United States, IMPROVE data could be biased. However, transport from other continents does not seem to be significant and does not contribute to the discrepancy. Indeed, dust transport from Africa seems correct as the relative error along the Gulf of Mexico is less than 25%, and dust concentration over the tropical Pacific is 10 times less than in the Southwest.

4.1.3. EMEP Data Set

[23] The concentration of PM10 sulfate has been monitored by the European Monitoring and Evaluation Program (EMEP) since 1977 at 102 stations spread across 27 countries in Europe [*Hjellbrekke*, 2005]. The monthly climatological concentrations are calculated by averaging valid data over the entire records. From July 2002 to July 2003, 13 European countries participated in the measurements of OC and BC [*EMEP*, 2004]. The one year measurement climatological values over Europe. The same technique used to grid the data from IMPROVE is also applied to EMEP data. We restrict the grid points to countries with operating EMEP sites. Figure 5 shows the comparison of observed and simulated aerosol concentrations as well as their relative difference. The model reproduces correctly the maximum concentrations of aerosol in central Europe and the decrease toward Scandinavia. For sulfate the relative error is less than 25% in most area. The large error in Switzerland is essentially due to an inability to resolve mountains flow, while in Russia the discrepancy is due to the scarcity of EMEP sites in eastern Europe. The results for annual mean $SO_4^=$ are better than reported in previous studies [*Kasibhatla et al.*, 1997; *Koch et al.*, 1999; *Barth et al.*, 2000; *Chin et al.*, 2002]. However, as we will show in section 5.2, this is due to compensating errors between winter and summer. For carbonaceous aerosols, Figure 5 seems to indicate errors of a factor 2 to 5 over northern Germany. However, the low number of sites tends to exaggerate the discrepancy.

4.2. Aerosol Optical Depth

4.2.1. Satellite Data

[24] Satellite measurements of backscattering radiance allow the retrieval of aerosol properties at the global or near-global scale. Some instruments have been rertrieving AOD since the late 1970s. *Myhre et al.* [2004b] have compared such data sets and found as much as a factor 2 differences between them. The AOD values from the advanced very high resolution radiometer (AVHRR) with a two-channel algorithm developed by *Mishchenko et al.* [1999] correspond to the middle to low range of retrieved values. With this algorithm, *Geogdzhayev et al.* [2002] have retrieved AOD over the ocean from 1982 to 2000. As stratospheric aerosols increased the AOD globally after the eruptions of El Chichón (March 1982) and Mount Pinatubo (June 1991), *Geogdzhayev et al.* [2004] used a stratospheric aerosol data from the Stratospheric Aerosol and Gas Experiment (SAGE) instrument to constrain the AVHRR retrieval algorithm. Figure 6 compares the time series of mean AOD over oceans retrieved from AVHRR data with CM2.1 values with and without volcanic aerosols. The model correctly reproduces the increase of total AOD after the two major eruptions, followed by a slow decrease as aerosols are removed from the atmosphere. The maximum contribution to the global average AOD from volcanoes, after the eruptions of El Chichón and Pinatubo reached 0.09 and 0.13, respectively. These values represent 35% and 47% respectively of the total optical depth. As there were no major volcanic eruptions after Mount Pinatubo, the contribution is negligible after 1996. In 2000, the global mean AOD value over ocean is 0.15 for AVHRR and 0.14 for CM2.1. The mean bias of the simulated global AOD (tropospheric and stratospheric volcanic aerosols) versus the observations from AVHRR is −5% over 19 years with values ranging from less than −0.1% in 1994 to −16% in 1983. After 1996, the difference is less than

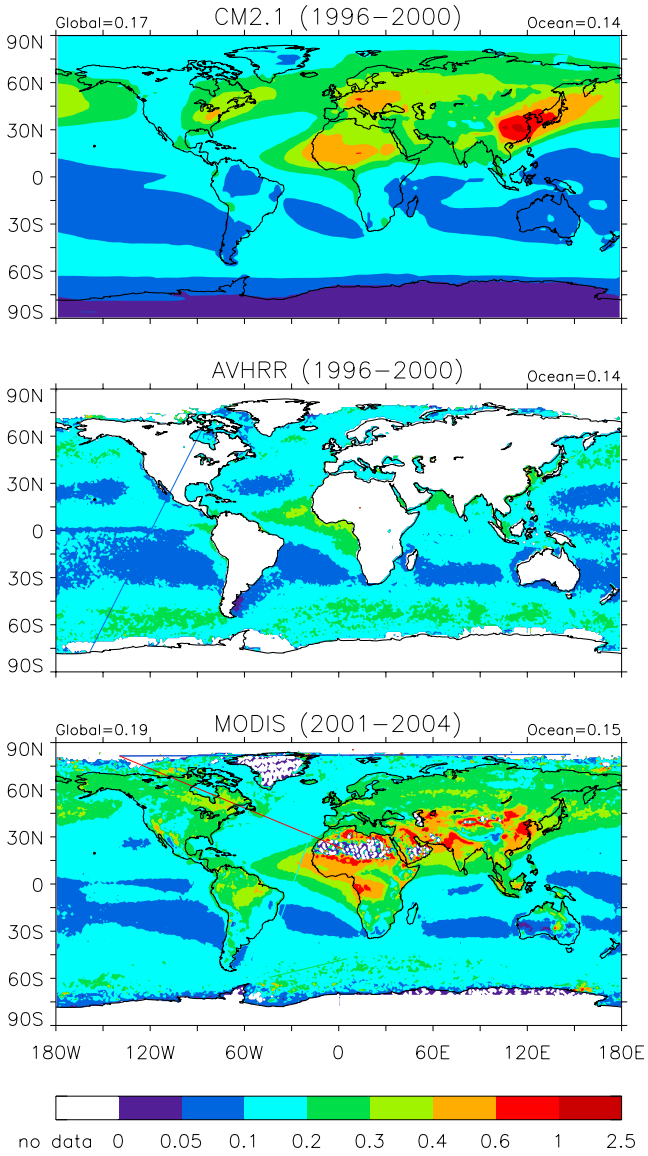

Figure 7. Comparison of annual mean optical depth at 550 nm (top) simulated with CM2.1 (1996–2000 average), (middle) retrieved from AVHRR (1996–2000 average), and (bottom) from MODIS (2002–2004 average). The global and ocean mean AOD are indicated over each panel on the left and right, respectively, except for AVHRR AOD in Figure 7 (middle), for which only ocean mean AOD is provided.

−5%. Such good agreement at the global scale masks differences of opposite signs at the regional scale. These regional differences can be seen in Figure 7, which compares AOD distributions from CM2.1 and satellite retrievals. The comparison indicates that AOD is overestimated in the northern mid latitude oceans and underestimated in the southern ocean. In the tropical and subtropical oceanic regions the model underestimates the AOD by less than 50%.

[25] Since 2000, several platforms have been launched with onboard instruments dedicated to aerosols. Among them, the Moderate Resolution Imaging Spectroradiometer (MODIS) instrument retrieves aerosol properties over the oceans [*Tanré et al.*, 1997] and land [*Kaufman et al.*, 1997], in particular the AOD at 550 nm. The MODIS AOD are averaged from January 2001 to December 2004. As described by *Horowitz* [2006], the aerosol distribution is simulated one year per decade and the difference of aerosol burden from one decade to the next varies by 10% or less. So, the different averaging periods (1996–2000 for CM2.1, 2001–2004 for MODIS) should not have a large impact on our comparison. The MODIS mean AOD value is 0.15 over ocean and 0.19 globally. The corresponding values for CM2.1 are 0.14 and 0.17. These numbers confirm that CM2.1 reproduces correctly the observed AOD at the global scale. Also, the comparison in Figure 7 with MODIS AOD confirms that the agreement at the global scale results from discrepancies of opposite sign at the regional scale. However, the discrepancies with MODIS data are less pronounced over ocean than with AVHRR data. MODIS data further indicate that the larger errors are located over land: in particular, at midlatitude over industrialized countries and in the tropics over biomass burning regions.

4.2.2. Sun Photometer Data

[26] Uncertainties associated with satellite retrievals are close to the background values (i.e., 0.05). Therefore it is useful to compare AOD with accurate measurements from ground-based instruments. The Aerosol Robotic Network (AERONET) directly measures AOD [*Holben et al.*, 2001] with a world-wide network of Sun photometers that are representative of different aerosol regimes. As the instruments are well calibrated and the data are screened for clouds, the precision reaches 0.01 [*Holben et al.*, 2001]. Figure 8 shows the comparison between simulated and measured climatological AOD at 102 sites. The correlation between the simulated and observed values is 0.6. The geographical distribution of the relative difference indicates a clear latitudinal gradient, which confirms the results of our comparison with satellite data in section 4.2.1. Figure 8 shows three distinct types of behavior of the aerosol distribution in CM2.1: (1) in polluted regions of the Northern Hemisphere, the AOD is overestimated by a factor 2; (2) in the tropical North Atlantic, the AOD is reproduced to within 25%; and (3) in biomass burning regions of South America and South East Asia, the AOD is underestimated by a factor 2. Unfortunately, there are no AERONET sites in the southern ocean to confirm that CM2.1 is underpredicting the AOD.

5. Regional Analysis With Combined Data Sets

[27] In this section we evaluate the seasonal variation of aerosol concentration and optical depth over regions characterized by a range of aerosol conditions. In the previous section, it was shown that there appears to be an equal amount of error in AOD associated with assumed optical properties and with simulated aerosol concentration. In order to quantify the relative importance of both errors for different aerosol conditions, we show the measurements of AOD and surface concentration at the same or close-by sites. Over industrial regions such as Europe and North America, where AOD is dominated by hygroscopic $SO_4^=$, we also show the mass extinction coefficient, aerosol burden and relative humidity. As the mass extinction coefficient

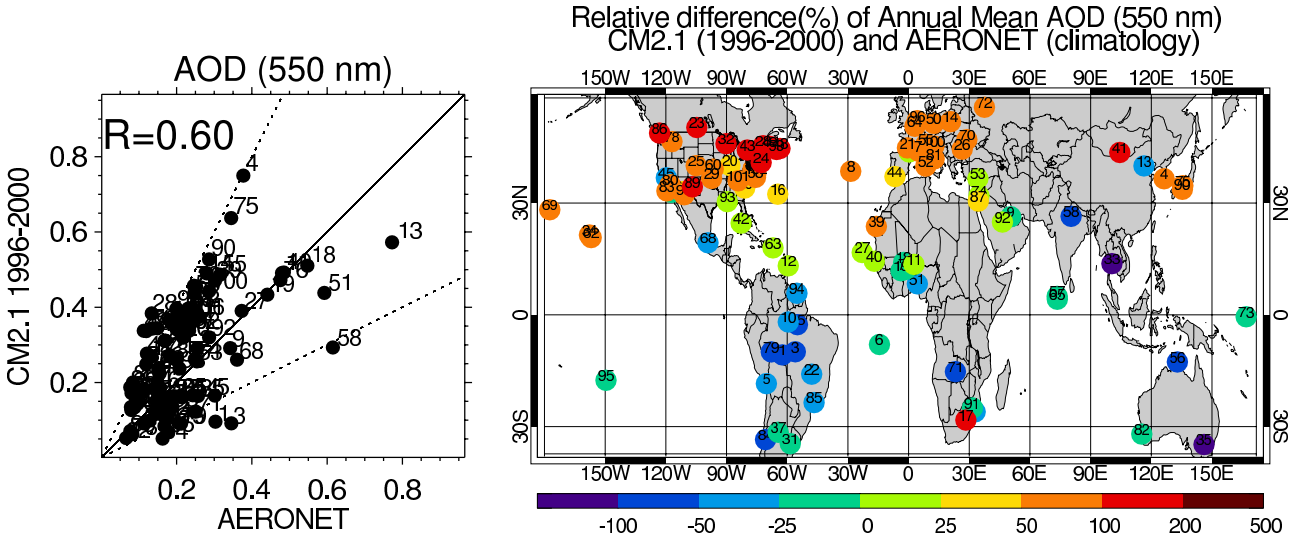

Figure 8. (left) Comparison of simulated (CM2.1, 1996–2000) and measured (AERONET, climatology) annual AOD at 550 nm at 102 locations and (right) relative difference, at each location, of simulated and observed AOD. The solid line in Figure 8 (left) indicates the 1:1 line, and the dashed lines are 2:1 and 1:2.

(α_e) is a nonlinear function of the relative humidity, its correlation with the frequency of occurrence of high values of RH provides useful information on the impact of hygroscopic growth on AOD. Unfortunately, no such statistics have been archived, and only the monthly mean RH is available. However, as α_e increases exponentially with RH, even a few occurrences of high RH (i.e., greater than 95%) will cause an increase of monthly mean α_e but not necessarily of RH. On the other hand, if RH deviates little from its monthly mean, the mass extinction coefficient should have seasonal variations similar to RH. In other words, the comparison of monthly mean RH and mass extinction coefficients allows the impact of high RH on AOD to be determined, and whether the mass extinction coefficient values are realistic. During the dry season, α_e approaches the value for dry aerosol given in Table 1. For aerosols located in a well mixed boundary layer, the surface concentration is proportional to the column burden, while in the case of elevated aerosol layers, there may be little correlation between surface concentrations and column burden or AOD.

5.1. North America

[28] Figure 9 shows the seasonal variation of monthly mean (1996–2000) AOD, mass extinction coefficient of sulfate (α_{SO4}), mass burden of $SO_4^=$, RH at 925 hPa, and surface concentration of aerosols at 6 AERONET surface sites selected to represent distinct regions of North America: the Northwest (Rimrock, Montana), the Southwest (Sevilleta, New Mexico), the Midwest (Bondville, Illinois), the South (CART site, Oklahoma), the Southeast (Columbia, South Carolina), and the Northeast (GSFC, Greenbelt, Maryland). The surface concentrations of $SO_4^=$, OC, BC and fine dust at the AERONET sites correspond to the closest grid point of the IMPROVE data gridded following the method explained in section 4.1.2. At all sites, sulfate makes the greatest contribution to model AOD, ranging from 70% to 90%. This is in agreement with other modeling studies [e.g., *Chin et al.*, 2002; *Takemura et al.*, 2002; *Reddy et al.*, 2005]. However, the values of α_{SO4} in CM2.1 exceed the values used by *Chin et al.* [2002] by a factor 2 to 4 over the United States. Their values vary from 5 $m^2\ g^{-1}$ in the Southwest to 16 $m^2\ g^{-1}$ in the Northeast, as compared to 20 $m^2\ g^{-1}$ (CART site) and 27 $m^2\ g^{-1}$ (GSFC) for CM2.1.

[29] The largest value of AOD for all sites is observed in the Northeast at GSFC in July and is reproduced by CM2.1 within 35%. The total monthly AOD is typically overestimated, with the largest discrepancy in spring in the Northeast (by up to a factor of 3 at GSFC in April) and the lowest in summer. The simulated AOD at all sites show a distinct peak in April, which is not observed, except in the Northwest at Rimrock. This April maximum is also apparent in α_{SO4} but not in the column burden or RH at 925 hPa. Therefore this discrepancy can be attributed to the occasional occurrence of high RH values and the treatment of hygroscopic growth for $SO_4^=$. In summer, the monthly mean RH is the lowest and CM2.1 reproduces the AOD to within one standard deviation of the daily AERONET data, although the surface concentration is overestimated. This would indicate that the simulated aerosols are not well mixed in the boundary layer and are concentrated near the surface. Alternatively, RH could be underestimated and the model AOD agrees with the observations because sulfate burden is overestimated. A comparison of RH values with observations is required to decide among the two alternatives. In winter the surface concentration is generally underestimated but the AOD is overestimated, while α_{SO4} and RH have maximum values. This suggests that values of α_{SO4} greater than 30 $m^2\ g^{-1}$ are excessive and more than compensate for the low simulated value of $SO_4^=$ concentration. In September the values of RH and α_{SO4} reach their minimum. As opposed to spring, it does not seem that in the fall there is a significant occurrence of high RH values, as both curves for α_{SO4} and RH have the same monthly variation in Figure 9. Also, at the midwestern and eastern

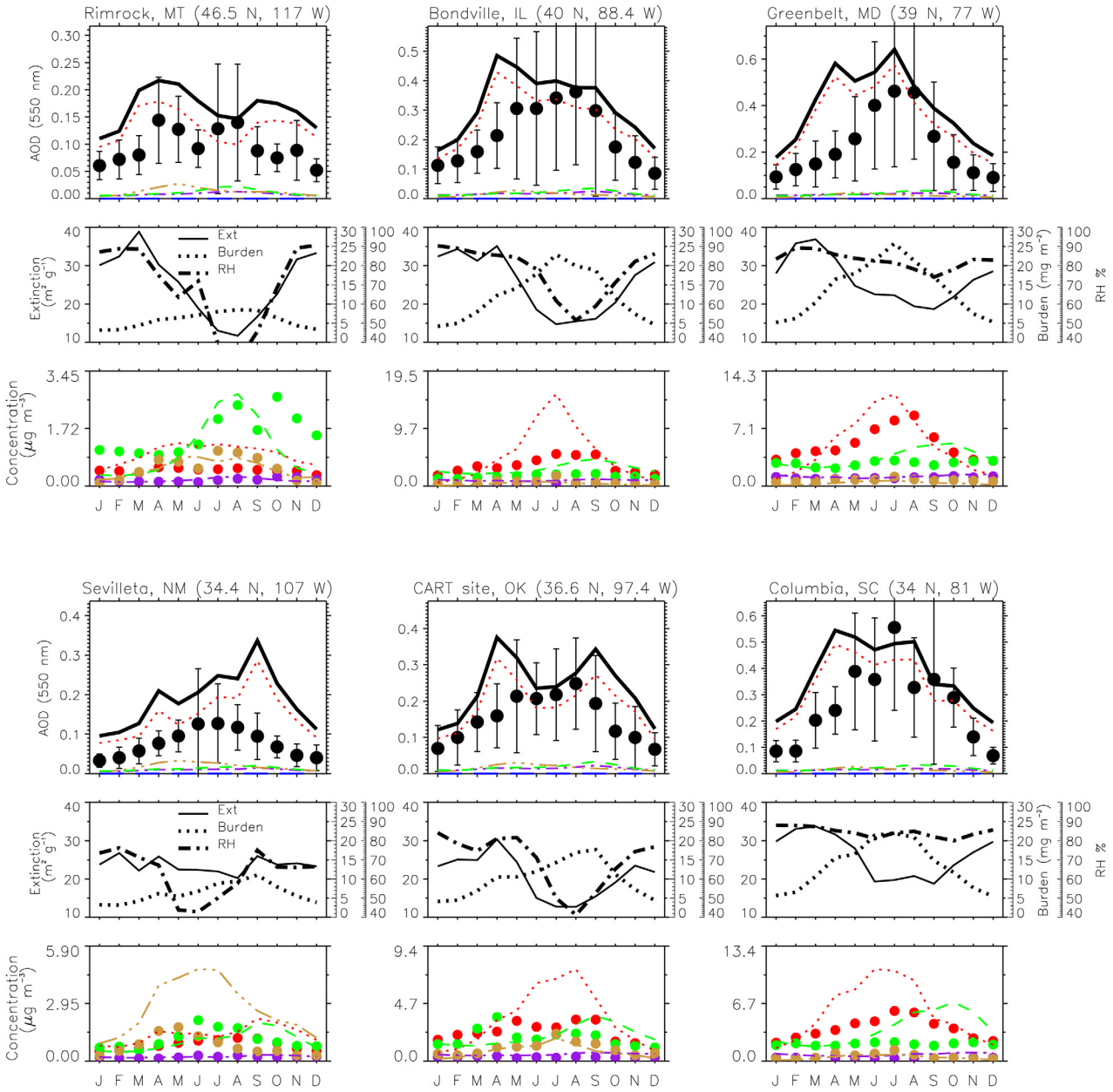

Figure 9. Comparison of monthly mean simulated aerosol optical depth at 550 nm (top plot for each location, lines) with AERONET data (black dots, daily standard deviation indicated by vertical lines) and surface concentrations (bottom plot for each location, lines) with interpolated IMPROVE data (dots) at six sites over North America. The middle plots show the column mass extinction efficiency of $SO_4^=$ (Ext, solid line, range from 10 to 40 $m^2\ g^{-1}$), column burden of $SO_4^=$ (Burden, dots, range from 0 to 30 mg m^{-2}), and relative humidity at 925 hPa (RH, dash-dotted line, range from 40 to 100%). Each aerosol component is indicated with its own color: total (thick black line), sulfate (red dotted line), organic (green dashed line), black carbon (violet dash-dotted line), dust (yellow dash-dot-dot-dotted line), and sea salt (blue dash-dot-dotted line).

sites the surface concentration of $SO_4^=$ is well reproduced and the AOD is accurate to within one standard deviation of daily AERONET data.

5.2. Europe

[30] Figure 10 shows the seasonal variation of (1996–2000) AOD, α_{SO4}, $SO_4^=$ mass burden, RH at 925 hPa, and surface concentration at eight representative AERONET sites in Europe. The observed surface values correspond to the values at the closest grid point of the EMEP data gridded with the method described in section 4.1.3. As for North America in Figure 9, CM2.1 produces a peak AOD in April which is not observed in the AERONET data; in winter the hygroscopic growth of $SO_4^=$ again compensates

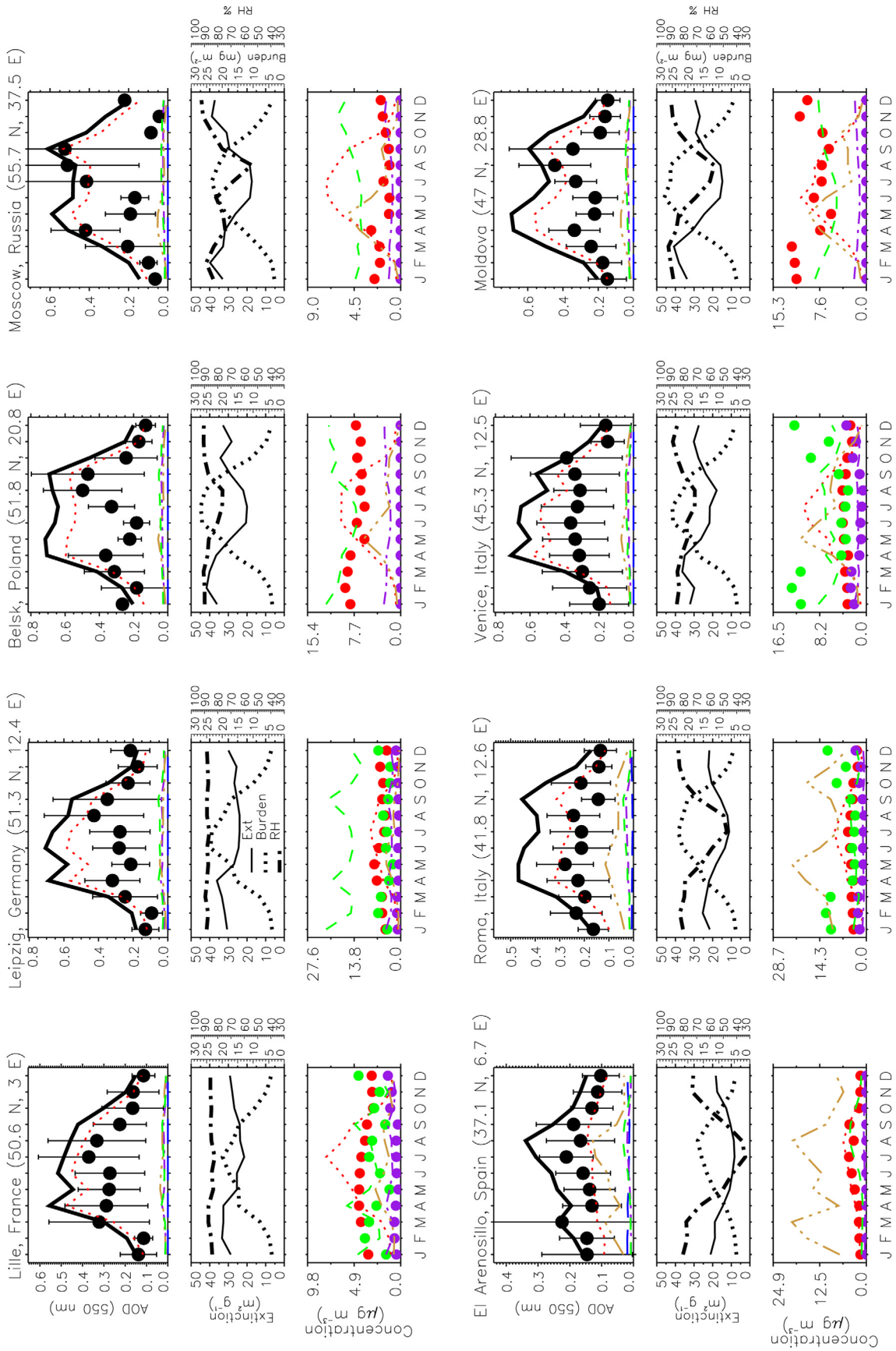
Lille, France (50.6 N, 3 E)
Leipzig, Germany (51.3 N, 12.4 E)
Belsk, Poland (51.8 N, 20.8 E)
Moscow, Russia (55.7 N, 37.5 E)
El Arenosillo, Spain (37.1 N, 6.7 E)
Roma, Italy (41.8 N, 12.6 E)
Venice, Italy (45.3 N, 12.5 E)
Moldova (47 N, 28.8 E)
AOD (550 nm)
Extinction (m² g⁻¹)
Burden (mg m⁻²)
Concentration (μg m⁻³)
RH %
Ext
Burden
RH
J F M A M J J A S O N D

Figure 10

for the largely underestimated surface concentration. Contrary to Figure 9, several European sites in the northern countries have RH at 925 hPa above 85% and the AOD is overestimated by more than a factor 2. The α_{SO4} values have more pronounced extrema in Europe: from 11 m^2 g^{-1} in Spain (El Arenosillo site) to 42 m^2 g^{-1} in Germany (FT Leipzig site). The annual mean values of α_{SO4} are higher in Europe and range from 19 m^2 g^{-1} to 31 m^2 g^{-1} for the same two sites, respectively. The best agreement in both AOD and surface concentration is in the drier cities of southern Europe (El Arenosillo). Figure 10 shows that the $SO_4^=$ concentration is generally overestimated in summer and underestimated in winter. These errors of opposite sign compensate one another in the annual mean, which is reproduced to within 25% of EMEP data, as shown in Figure 5. It is interesting to note that the excessive AOD in April simulated with CM2.1 is not confined to North America but appears also in Figure 10 over Europe. Given that the similar peak in April also dominates the seasonal cycle of α_{SO4} but not the cycles of the monthly mean RH at 925 hPa and column burden of $SO_4^=$, this April peak of AOD is most likely due to occasional occurrence of high RH like in North America. In Europe, the contribution to AOD from dust is comparable to that from $SO_4^=$ over sites influenced by Saharan dust. Although the dust concentration decreases rapidly with increasing distance from Sahara, it is still comparable to the concentration of other aerosols even as far as Moscow. As EMEP does not retrieve dust concentration, it is not possible to confirm such long-range transport of dust to high latitudes. Organic aerosols have also higher concentrations in Europe than in North America, and have higher concentration in winter than in summer. These characteristics appear to be correctly simulated at the sites with measurements of OC concentration.

5.3. Biomass Burning Regions

[31] Large-scale biomass burning in the tropics produces high amounts of smoke aerosols with AOD reaching its maximum during the dry season. Figure 11 shows the comparison of AOD at four AERONET sites in tropical burning regions. There is a peak in the activity of biomass burning from August through September at three of the sites [*Holben et al.*, 1996]: Alta Floresta in South America, and Mongu and Skukuza in South Africa. At the fourth selected site, Ilorin in West Africa, fires intensify from December to February [*Smirnov et al.*, 2002a]. Figure 11 shows that CM2.1 underestimates the peak values of AOD by a factor of 2 to 5 at all sites. Furthermore, OC contribution to AOD is equivalent or lower than the sulfate contribution at most sites. This does not correspond to previous analyses of AERONET data at these sites [e.g., *Eck et al.*, 1999; *Holben et al.*, 2001], and other model studies [e.g., *Chin et al.*, 2002; *Reddy et al.*, 2005]. However, the peak in simulated OC optical depth coincides with the observed maximum AOD at all sites, except Ilorin. This would indicate that the timing of emission is properly simulated. Furthermore, Table 2 would suggest that the global OC burden is within the range of other model values. These other model studies have shown that the emission rates are underestimated. All of this suggests that the large underestimation of OC optical depth is due to both the emission rates and optical properties. As the environment is dry during the biomass burning season, hygroscopicity should have a minimal impact on AOD. So the discrepancies in Figure 11 are mostly due to the value of the mass extinction coefficient of OC, which has been inadvertently converted to organic matter (OM). Converting back to OC extinction coefficient, would improve the comparisons.

5.4. Dusty Environments

[32] Dust sources are located in arid regions and preferentially in topographic depressions [*Prospero et al.*, 2002]. Satellite images show frequent dust plumes that are several thousands of kilometers long, moving from their sources to remote oceans. The most frequent plumes are from West Africa and are transported over the North Atlantic to the Caribbean. Figure 12 shows the comparison of AOD at six AERONET sites in dusty environments. The comparisons of surface concentration with existing data is also shown. At Barbados, the model reproduces the observed AOD within one standard deviation. In agreement with *Smirnov et al.* [2000], the seasonal variation of AOD is well correlated with the surface concentration of dust. However, the model lags by one month the observed maximum in June for both the AOD and surface concentration. Cape Verde Island and Banizoumbou (Niger) are located downwind of major dust sources of West Africa. The model reproduces the seasonal cycle of surface dust concentration but the amplitude is slightly overestimated. At both sites, the simulated monthly mean extinction is usually within the standard deviation of the measurements. However, *Holben et al.* [2001] have indicated that, in late winter/early spring, biomass burning aerosols contribute as much as dust to the AOD. This contribution is not present in the model. We explained the low contribution of biomass burning aerosols to AOD in the previous section. At Sede Boker (Israel), the model exhibits a springtime maximum associated with dust loading. During the following seasons, there is an equal contribution from dust and sulfate extinctions. These results are in agreement with the analysis of AERONET data by *Pinker et al.* [1997] and other model studies [e.g., *Chin et al.*, 2002, *Reddy et al.*, 2005]. Furthermore, Figure 12 shows that the observed surface concentration of dust is reproduced at Sede Boker within 50%. At Bahrain, the seasonal variation of AOD is dominated by dust, although sulfate contribution is not negligible especially in summer. This is consistent with

Figure 10. Comparison of monthly mean simulated aerosol optical depth at 550 nm (top plot for each location, lines) with AERONET data (black dots, daily standard deviation indicated by vertical lines) and sulfate surface concentrations (bottom plot for each location, lines) with interpolated EMEP data (dots) at eight sites over Europe. The middle plots show the column mass extinction efficiency of $SO_4^=$(solid line, range from 10 to 40 m^2 g^{-1}), column burden of $SO_4^=$ (dots, range from 0 to 30 mg m^{-2}), and relative humidity at 925 hPa (RH, dash-dotted line, ranging from 40 to 100%). Each aerosol component is indicated with its own color: total (thick black line), sulfate (red dotted line), organic (green dashed line), black carbon (violet dash-dotted line), dust (yellow dash-dot-dot-dotted line), and sea salt (blue dash-dot-dotted line).

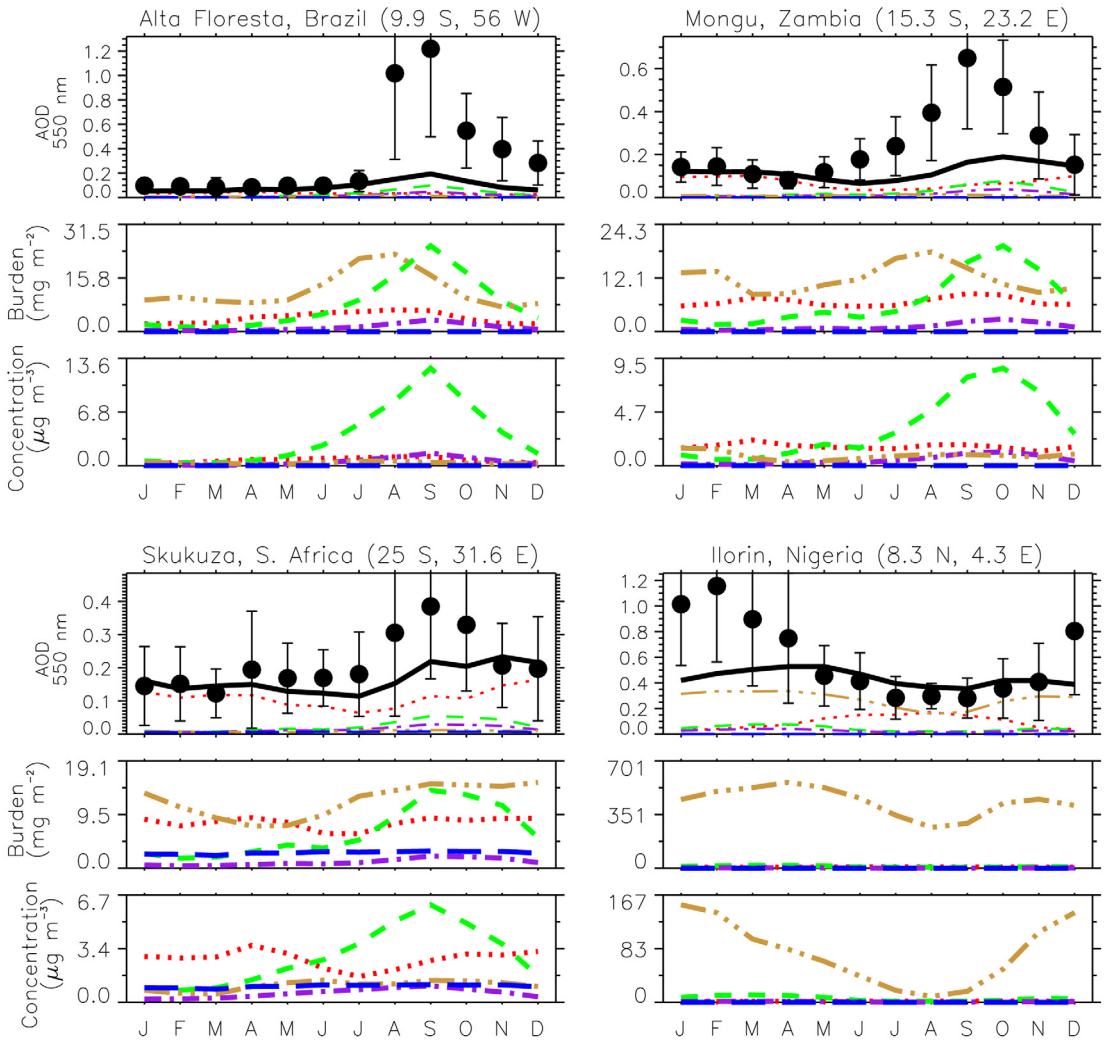

Figure 11. Comparison of modeled (black line for all components and colored lines for each component) and observed (black dots for AOD and colored dots for aerosol component surface concentration; vertical lines show daily standard deviation) AOD at 550 nm (top plot for each location), mass column (mg m^{-2}, middle plot for each location), and surface concentration (μg m^{-3}, bottom plot for each location) of each aerosol type (sulfate, red dotted line; organic, green dashed line; black carbon; violet, dash-dotted line; dust, yellow dash-dot-dot-dotted line; sea salt, blue dash-dot-dotted line) at six AERONET sites located over biomass burning regions in South America (Alta Floresta), western Africa (Ilorin), and southern Africa (Mongu and Skukuza).

the analysis of AERONET data by *Smirnov et al.* [2002b]. Indeed, during occasional nondusty days, they detected the presence of hygroscopic aerosols. At Dalanzadgad (Mongolia), the AOD is overestimated by a factor of 2, with almost equal contributions from sulfate and dust. The observed AOD is well reproduced by dust extinction alone, with a springtime maximum. However, as sulfate is practically constant throughout spring and summer, the simulated AOD shows a broad summer maximum. On the basis of the values of Angstrom parameter from AERONET data at Dalanzadgad, *Holben et al.* [2001] indicated that except for spring, fine particles make the dominant contribution to the AOD. In spring the low values of the Angstrom parameter suggest that dust dominates. Another analysis of sky radiometer data collected in various arid regions of China by *Uchiyama et al.* [2005] supports this conclusion, suggesting that contribution of dust particles to AOD in spring is over 70%. On the basis of these studies sulfate extinction is largely overestimated in spring. The model results by *Chin et al.* [2002] showed similar overestimation of AOD and a shift of the maximum toward summer due to the contribution from sulfate.

5.5. Maritime Environments

[33] Figure 13 shows the comparison of AOD at AERONET sites dominated by marine aerosols (i.e., sea salt and natural sulfate from oxidation of dimethylsulfide) and long-range transport of aerosols from continents. At all of these sites, sulfate dominates the AOD in CM2.1, although sea salt has the largest concentration at the surface at all sites

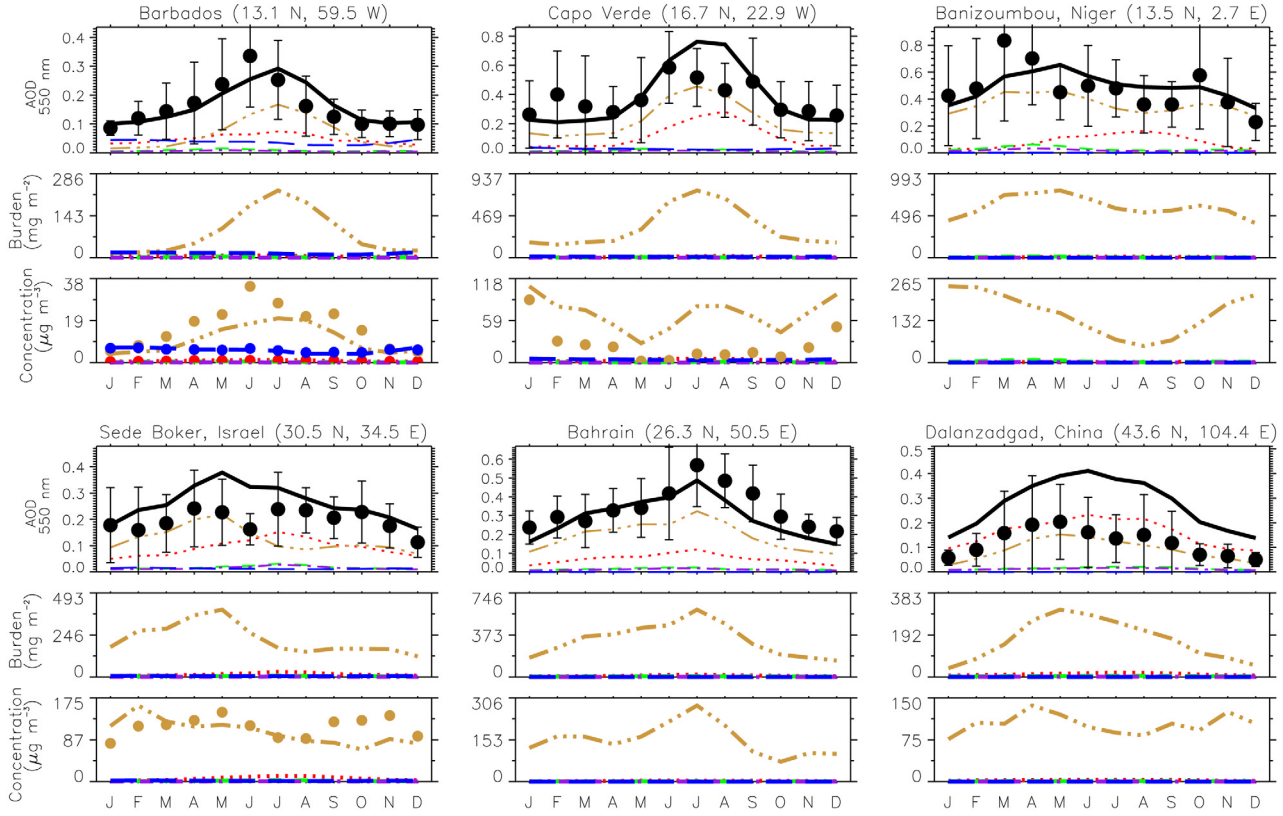

Figure 12. Comparison of modeled (black line for all components and colored lines for each component) and observed (black dots for AOD and colored dots for aerosol component surface concentration; vertical lines show standard deviation) AOD at 550 nm (top plot for each location), column loading (mg m^{-2}, middle plot for each location) and surface concentration (μg m^{-3}, bottom plot for each location) of each aerosol type (sulfate, red dotted line; organic, green dashed line; black carbon, violet dash-dotted line; dust, yellow dash-dot-dot-dotted line; sea-salt, blue dash-dot-dotted line) at six AERONET sites located in dusty environments in the North Atlantic (Barbados and Cape Verde), West Africa (Banizoumbou), Israel (Sede Boker), Arabian Peninsula (Bahrain), and Mongolia (Dalanzadgad). The surface concentration of dust is compared at Barbados with University of Miami data, at Cape Verde with measurements by *Chiapello et al.* [1995], and at Sede Boker with data from *Offer and Goossens* [2001]. The sea-salt concentration at Barbados has been measured by the University of Miami.

and the largest column burden at Nauru and Tahiti. This discrepancy can be explained by the absence in CM2.1 of hygroscopic growth for sea salt beyond 80% RH, while sulfate is allowed to grow up to 100% RH. The simulated AOD is within the standard deviation of AERONET data, except at the sites in the North Pacific where the AOD is overestimated by up to a factor 2. The comparison of sea-salt concentration at Nauru, Midway, and Hawaii islands indicates that CM2.1 underestimates its value by at least a factor 2. Assuming a well mixed maritime boundary layer, the sea-salt contribution to AOD should be more than a factor 2 considering also the lack of hygroscopic growth beyond 80% RH. In that case, the AOD would be overestimated at all sites by an equivalent amount. Given that simulated $SO_4^=$ concentration is within a factor 2 of the data (Figure 13 and section 4.1.1), it seems that the mass extinction coefficient of hygroscopic $SO_4^=$ is also overestimated in maritime environments. Therefore the excess of hygroscopic growth of $SO_4^=$ in the model compensates for the underprediction of sea-salt burden such that the simulated AOD reproduced most of the AERONET data.

6. Conclusions

[34] This study evaluates the strength and weakness of aerosol distributions and AOD used to simulate climate change with the GFDL coupled model CM2.1. The concentrations of sulfate, organic carbon, black carbon and dust were simulated with the MOZART 2 model [*Horowitz*, 2006], while the sea-salt concentration is from *Haywood et al.* [1999]. Our evaluation is based on comparisons at the global and regional scales with ground-based and remote sensing observations dating from 1980. The comparisons include aerosol surface concentrations measured over islands by the University of Miami, over the United States by the IMPROVE monitoring network, and over Europe by the EMEP monitoring instruments. The aerosol optical depth is compared with AVHRR and MODIS satellite data, and ground-based Sun photometer data from AERONET.

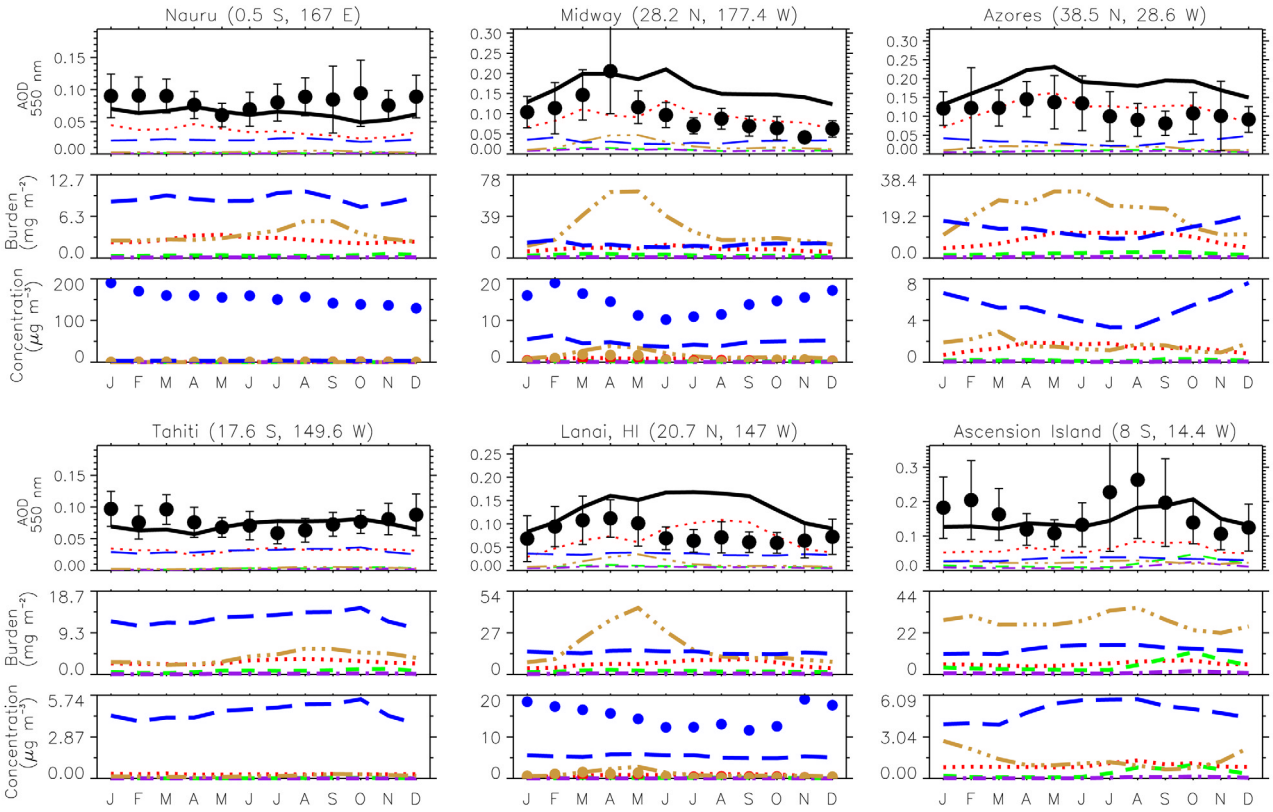

Figure 13. Comparison of modeled (black line for all components and colored lines for each component) and observed (black dots for AOD and colored dots for aerosol component surface concentration; vertical lines show standard deviation) AOD at 550 nm (top plot for each location), column loading (mg m^{-2}, middle plot for each location), and surface concentration (μg m^{-3}, bottom plot for each location) of each aerosol type (sulfate, red dotted line; organic, green dashed line; black carbon, violet dash-dot line; dust, yellow dash-dot-dot-dotted line; sea salt, blue dash-dot-dotted line) at six AERONET sites located in maritime environments in the South Pacific (Nauru, Tahiti), North Pacific (Midway, Lanai), North Atlantic (Azores), and South Atlantic (Ascension Island). For Nauru, Midway, and Lanai the measured concentrations of sulfate (red dots) and dust (yellow dots) are shown in the bottom plots. The surface concentration of sulfate, dust, and sea salt is compared with data from the University of Miami at Nauru and Midway [*Prospero et al.*, 2003]. At the AERONET site in Lanai we compare with the University of Miami data at Oahu.

We also compare our results with previous modeling studies.

[35] The individual evaluation of each aerosol component shows the following strengths and weakness.

[36] 1. The first component is sulfate: The annual mean surface concentration is reproduced within a factor 2 with values ranging from 0.05 μg m^{-3} in remote marine atmosphere to 13 μg m^{-3} in polluted regions. In general, the simulated concentrations are overpredicted in summer and underpredicted in winter. Sulfate mass column and zonal mean profiles are comparable to other studies, although the global mean burden is about 15% higher. The major discrepancy compare with observations is in the amplitude and seasonal variation of sulfate AOD. In some regions where sulfate dominates the aerosol extinction, the simulated optical depth is a factor of 2 or more higher than the observations during some months. In Europe and North America the aerosol optical depth is overestimated by up to a factor of 5 in April. In maritime environments, there is no apparent discrepancy of AOD, but this is because the dominant $SO_4^=$ contribution to AOD compensates for the underprediction of sea-salt burden. The global mean sulfate AOD is twice the value from other model studies. As the optical parameters are similar to these studies, we find that this discrepancy is due to the treatment of hygroscopic growth and the occurrence of very moist conditions. Sulfate is allowed to grow in our study up to 100% relative humidity while other models impose a somewhat arbitrary cutoff from 95% to 99% RH to distinguish haze particles from cloud droplets. In situ measurements by *Wulfmeyer and Feingold* [2000] indicate that maritime aerosols continue to grow at least to 98.5%. Laboratory measurements were also unable to measure growth beyond 98% RH. As the models have to extrapolate values up to 100% RH, large discrepancies may arise. As no statistics have been archived on the occurrence of model RH values greater than 95%, it is not possible to determine the exact impact of the simulated RH on the AOD. We suggest that the occurrence

of very high RH values in the model and the hygroscopic growth of sulfate at these RH values ought to be further investigated.

[37] The second component is organic and black carbon: The annual mean concentration is generally overestimated in polluted regions by up to a factor of 2. Other model studies indicate that carbonaceous aerosols are systematically underestimated, particularly for organic carbon. An exception is West Africa where other models show significant loadings of carbonaceous aerosols associated with biomass burning activities during the dry season while our results do not show any perturbation arising from such activities. The source of this discrepancy seems to be caused in part by the emission inventory in West Africa. Although the surface concentrations does not seem to systematically underestimate the observations, the global mean optical depth due to carbonaceous aerosols is a factor of 2 to 3 lower than reported by other studies. This is because of the error of specific extinction of OC, which differs from that in other modeling studies. Our value was inadvertently converted to organic matter. An additional effect could be the lack of hygroscopic growth of organic aerosols which could improve the comparisons under moist conditions.

[38] 3. The third component is dust: The annual mean dust concentration at the surface agrees with the observations to within a factor 2, except over Antarctica where it is underestimated by a factor of 5. Over that region, the concentrations are very low and this large discrepancy would not affect the optical depth substantially. The comparison of submicron dust concentration over the United States reveals that it is overestimated by up to a factor 10 in the dust source regions in the Southwest, but in the Northeast, the model reproduces to within 25% the observed surface concentration. Our analysis does not allow us to determine if the problem is related to the fraction of submicron particles assumed in the emission scheme, or related to the bulk emission rate in the Southwest. The most accurate comparison of AOD with satellite and ground-based measurements is obtained in regions and seasons where dust dominates the total extinction.

[39] 4. The fourth component is sea salt: The sea-salt surface concentrations are systematically underestimated by more than a factor of 2. The global burden is correspondingly in the low end of the range of values from other models. The optical depth in marine environments is generally within the standard deviation of the data or overestimated by less than a factor of 2. It is shown that the excessive extinction by sulfate compensates the largely underestimated contribution from sea salt to AOD. This compensation effect disappears over the southern oceans where high optical depths, observed from satellite, have been associated with high wind speeds emitting large amounts of sea salt. In that region the simulated optical depth is underestimated by a factor of 2.

[40] Overall, the concentrations of the different aerosols are within a factor 2 of the observed values, and have a tendency to be overestimated. It is possible that slightly higher rates of removal would improve the comparisons. The one exception is sea salt, which has concentrations that are a simple function of wind speed and which should be replaced with more realistic distributions.

[41] These results and the comparison with satellite data show that the relatively good agreement of global mean optical depth masks regional differences of opposite signs. Essentially, the larger than observed aerosol optical depth by sulfate compensates the lower contribution of OC and sea-salt aerosols. The largest discrepancies are over the northeast United States and Europe (AOD overestimated), biomass burning region and over the southern oceans (AOD underestimated).

[42] This analysis indicates that major improvements could be achieved by (1) reassessing the method by which hygroscopic growth is calculated at high relative humidities in CM2.1, and should include a thorough assessment of growth at RH between 95% and 100%, (2) using simulated sea-salt distributions from a transport model (e.g., MOZART 2), (3) correcting the error associated to the specific extinction coefficient of organics, (4) treating hygroscopic growth of organics, (5) better constraining the emissions in biomass burning regions.

[43] The influence of sulfate aerosol optical depth is particularly critical for climate models. Sulfate contributes the largest aerosol optical depth at most places, and exhibits strong hygroscopic growth especially at RH values greater than 85%. Thus it is imperative that model simulations be subject to stringent comparisons against laboratory and field observations of sulfate surface concentration and optical depth.

[44] **Acknowledgments.** We are grateful to Yi Ming, Vaughan Phillips, Shekar Reddy, and two anonymous reviewers for providing useful comments on the manuscript. We also thank Joseph M. Prospero and Dennis Savoie from the University of Miami for providing his data set of measurements of sulfate, dust, and sea-salt surface concentrations. We thank all the principal investigators of the 102 Sun photometers data federated to AERONET. We thank the Norwegian Institute for Air Research (NILU) for providing EMEP data and the Colorado State University for providing IMPROVE data. Finally, we wish to thank the developers of the NASA GES-DISC Interactive Online Visualization and Analysis Infrastructure (GIOVANNI), which greatly facilitated the extraction of MODIS data.

References

Barth, M., P. J. Rasch, J. T. Kiehl, C. M. Benkovitz, and S. E. Schwartz (2000), Sulfur chemistry in the National Center for Atmospheric Research Community Climate Model: Description, evaluation, features, and sensitivity to aqueous chemnistry, *J. Geophys. Res.*, *105*, 1387–1415.

Chiapello, I., G. Bergametti, L. Gomes, B. Chatenet, F. Dulac, J. Pimenta, and E. Santos Suares (1995), An additional low layer transport of Sahelian and Saharan dust over the north-eastern tropical Atlantic, *Geophys. Res. Lett.*, *22*, 3191–3194.

Chin, M., P. Ginoux, S. Kinne, O. Torres, B. N. Holben, D. N. Duncan, R. V. Martin, J. A. Logan, A. Higurashi, and T. Nakajima (2002), Tropospheric aerosol optical depth from the GOCART model and comparisons with satellite and Sun photometer measurements, *J. Atmos. Sci.*, *59*, 461–483.

Chung, S. H., and J. H. Seinfeld (2002), Global distribution and climate forcing of carbonaceous aerosols, *J. Geophys. Res.*, *107*(D19), 4407, doi:10.1029/2001JD001397.

Delworth, T. L., R. J. Stouffer, K. W. Dixon, M. J. Spelman, T. R. Knutson, A. J. Broccoli, P. J. Kushner, and R. T. Wtherald (2002), Review of simulations of climate variability and changes with the GFDL R30 coupled climate model, *Clim. Dyn.*, *19*, 555–574.

Delworth, T. L., et al. (2006), GFDL's CM2 global coupled climate models - Part 1: Formulation and simulation characteristics, *J. Clim.*, *19*(5), 643–674.

Dubovik, O., B. Holben, T. Eck, A. Smirnov, Y. J. Kaufman, M. D. King, D. Tanré, and I. Slutsker (2002), Variability of absorption and optical properties of key aerosol types observed in worldwide locations, *J. Atmos. Sci.*, *59*, 590–608.

Eck, T. F., B. N. Holben, J. S. Reid, O. Dubovik, A. Smironov, N. T. O'Neill, I. Slutsker, and S. Kinne (1999), Wavelength dependence of

the optical depth of biomass burning, urban, and desert dust aerosols, *J. Geophys. Res.*, *104*, 31,333–31,349.
European Monitoring and Evaluation Program (EMEP) (2004), Measurements of particular matter: Status report 2004, *Rep. 3/2004*, 64 pp., Norw. Inst. for Air Res., Kjeller.
Fitzgerald, J. W. (1975), Approximation formulas for the equilibrium size of an aerosol particle as a function of its dry size and composition and the ambient relative humidity, *J. Appl. Meteorol.*, *14*, 1044–1049.
Freidenreich, S. M., and V. Ramaswamy (1999), A new multiple-band solar radiative parameterization for general circulation models, *J. Geophys. Res.*, *104*, 31,389–31,409.
Genthon, C. (1992), Simulations of desert dust and sea-salt aerosols in Antarctica with a general circulation model of the atmosphere, *Tellus, Ser. B*, *44*, 371–389.
Geogdzhayev, I. V., M. I. Mishchenko, W. B. Rossow, B. Cairns, and A. A. Lacis (2002), Global two-channel AVHRR retrievals of aerosol properties over the ocean for the period of NOAA-9 observations and preliminary retrievals using NOAA-7 and NOAA-11 data, *J. Atmos. Sci.*, *59*, 262–278.
Geogdzhayev, I. V., M. I. Mishchenko, L. Liu, and L. Remer (2004), Global two-channel AVHRR aerosol climatology: Effects of stratospheric aerosols and preliminary comparisons with MODIS and MISR retrievals, *J. Quant. Spectrosc. Radiat. Transfer*, *88*, 47–59.
Geophysical Fluid Dynamics Laboratory Global Atmospheric Model Development Team (2004), The new GFDL global atmosphere and land model AM2-LM2: Evaluation with prescribed SST simulations, *J. Clim.*, *17*(24), 4641–4673.
Ginoux, P., M. Chin, I. Tegen, J. M. Prospero, B. Holben, O. Dubovik, and S.-J. Lin (2001), Sources and distributions of dust aerosols simulated with the GOCART model, *J. Geophys. Res.*, *106*, 20,255–20,273.
Goudie, A. S., and N. J. Middleton (2001), Saharan dust storms: Nature and consequences, *Earth Sci. Rev.*, *56*, 179–204.
Hansen, J. E., et al. (2002), Climate forcing in Goddard Institute for Space Studies SI2000 simulations, *J. Geophys. Res.*, *107*(D18), 4347, doi:10.1029/2001JD001143.
Haywood, J. M., and V. Ramaswamy (1998), Global sensitivity studies of the direct radiative forcing due to anthropogenic sulfate and black carbon aerosols, *J. Geosphys. Res.*, *103*(D6), 6043–6058.
Haywood, J. M., V. Ramaswamy, and L. J. Donner (1997), A limited-area model case study of the effects of sub-grid scale variations in relative humidity and cloud upon the direct radiative forcing of sulfate aerosol, *Geophys. Res. Lett.*, *24*, 143–144.
Haywood, J. M., V. Ramaswamy, and B. J. Soden (1999), Tropospheric aerosol climate forcing in clear-sky satellite observations over the oceans, *Science*, *283*, 1299–1301.
Hjellbrekke, A.-G. (2005), Data Report 2003 Acidfying and eutrofying compounds, *Rep. 3/2005*, 125 pp., Norw. Inst. for Air Res., Kjeller.
Holben, B. N., A. Setzer, T. F. Eck, A. Pereira, and I. Slutsker (1996), Effect of dry season biomass burning on Amazon Basin aerosol concentrations and optical properties, *J. Geophys. Res.*, *101*, 19,465–19,481.
Holben, B. N., et al. (1998), AERONET: A federated instrument network and data archive for aerosol characterization, *Remote Sens. Environ.*, *66*, 1–16.
Holben, B. N., et al. (2001), An emerging ground-based aerosol climatology: Aerosol optical depth from AERONET, *J. Geophys. Res.*, *106*, 12,067–12,097.
Horowitz, L. W. (2006), Past, present, and future concentrations of tropospheric ozone and aerosols: Methodology, ozone evaluation, and sensitivity to aerosol wet removal, *J. Geophys. Res.*, *111*, D22211, doi:10.1029/2005JD006937.
Horowitz, L. W., et al. (2003), A global simulation of tropospheric ozone and related tracers: Description and evaluation of MOZART, version 2, *J. Geophys. Res.*, *108*(D24), 4784, doi:10.1029/2002JD002853.
Kasibhatla, P., W. L. Chameides, and J. St. Hohn (1997), A three-dimensional global model investigation of seasonal variations in the atmospheric burden of anthropogenic sulfate aerosols, *J. Geophys. Res.*, *102*, 3737–3759.
Kaufman, Y. J., et al. (1997), Remote sensing of tropospheric aerosol from EOS-MODIS over the land using dark targets and dynamic aerosol models, *J. Geophys. Res.*, *102*, 17,051–17,067.
Kaufman, Y. J., D. Tanré, O. Dubovik, A. Karmieli, and L. A. Remer (2001), Absorption of sunlight by dust as inferred from satellite and ground-based measurements, *Geophys. Res. Lett.*, *28*, 1479–1482.
Kiehl, J. T., J. J. Hack, G. B. Bonan, B. A. Boville, D. L. Williamson, and P. J. Rasch (1998), The National Center for Atmospheric Research Community Climate Model: CCM3, *J. Clim.*, *11*, 1131–1149.
Koch, D., D. Jacob, I. Tegen, D. Rind, and M. Chin (1999), Tropospheric sulfur simulations and sulfate direct radiative forcing in the GISS GCM, *J. Geophys. Res.*, *104*, 23,799–23,823.
Lin, S.-J. (2004), A "vertically Lagrangian" finite-volume dynamical core for global models, *Mon. Weather Rev.*, *132*(10), 2293–2307.
Liousse, C., J. E. Penner, C. Chuang, J. J. Walton, H. Eddleman, and H. Cachier (1996), A global three-dimensional model study of carbonaceous aerosols, *J. Geophys. Res.*, *101*, 19,411–19,432.
Lovett, R. S. (1978), Quantitative measurements of airborne sea salt in the North Atlantic, *Tellus*, *20*, 358–364.
Malm, W. C., J. F. Sisler, D. Huffman, R. A. Eldred, and T. A. Cahill (1994), Spatial and seasonal trends in particle concentration and optical extinction in the United States, *J. Geophys. Res.*, *99*, 1347–1370.
Ming, Y., V. Ramaswamy, P. Ginoux, and L. H. Horowitz (2005), Direct radiative forcing of anthropogenic organic aerosol, *J. Geophys. Res.*, *110*, D20208, doi:10.1029/2004JD005573.
Mishchenko, M. I., I. V. Geogdzhayev, L. Liu, J. A. Ogren, and A. A. Lacis (1999), Aerosol retrievals over the ocean by use of channels 1 and 2 AVHRR data: Sensitivity analysis and preliminary results, *Appl. Opt.*, *38*, 7325–7341.
Myhre, G., F. Stordal, T. F. Berglen, J. Sundet, and I. S. A. Isaksen (2004a), Uncertainties in the radiative forcing due to sulfate aerosols, *J. Atmos. Sci.*, *61*, 485–498.
Myhre, G., et al. (2004b), Intercomparison of satellite retrieved aerosol optical depth over the ocean, *J. Atmos. Sci.*, *61*, 499–513.
Offer, Z. Y., and D. Goosens (2001), Ten years of aeolian dust dynamics in a desert region (Negev desert, Israel): Analysis of airborne dust concentration, dust accumulation and the high-magnitude dust events, *J. Arid Environ.*, *47*, 211–249.
Patterson, E. M., D. A. Gillette, and B. H. Stockton (1977), Complex index of refraction between 300 and 700 nm for Saharan aerosols, *J. Geophys. Res.*, *82*, 3153–3160.
Penner, J. E., et al. (2001), Aerosols, their direct and indirect effects, in *Climate Change 2001: The Scientific Basis. Contribution of Working Group I to the Third Assessment Report of the Intergovernmental Panel on Climate Change*, pp. 289–348, Cambridge Univ. Press, New York.
Pinker, R. T., R. A. Ferrare, A. Karnieli, T. O. Aro, Y. J. Kaufman, and A. Zangvil (1997), Aerosol optical depths in a semiarid region, *J. Geophys. Res.*, *102*, 11,123–11,137.
Prospero, J. M. (1996), The atmospheric transport of particles to the ocean, in *Particle Flux in the Ocean*, edited by V. Ittekkot et al., *SCOPE Rep., 57*, pp. 19–52, John Wiley, Hoboken, N. J.
Prospero, J. M., P. Ginoux, O. Torres, S. Nicholson, and T. Gill (2002), Environmental characterization of global sources of atmospheric soil dust derived from the Nimbus 7 total ozone mapping spectrometer (TOMS) absorbing aerosol product, *Rev. Geophys.*, *40*(1), 1002, doi:10.1029/2000RG000095.
Prospero, J. M., D. Savoie, and R. Arimoto (2003), Long-term record of nss-sulfate and nitrate in aerosols on Midway Island, 19812000: Evidence of increased (now decreasing?) anthropogenic emissions from Asia, *J. Geophys. Res.*, *108*(D1), 4019, doi:10.1029/2001JD001524.
Ramachandran, S., V. Ramaswamy, G. L. Stenchikov, and A. Robock (2000), Radiative impact of the Mount Pinatubo volcanic eruption: Lower stratospheric response, *J. Geophys. Res.*, *105*, 24,409–24,429.
Ramaswamy, V., et al. (2001), Radiative forcing of climate change, in *Climate Change 2001: The Scientific Basis. Contribution of Working Group I to the Third Assessment Report of the Intergovernmental Panel on Climate Change*, pp. 349–416, Cambridge Univ. Press, New York.
Reddy, M. S., and O. Boucher (2004), A study of the global cycle of carbonaceous aerosols in the LMDZT general circulation model, *J. Geophys. Res.*, *109*, D14202, doi:10.1029/2003JD004048.
Reddy, M. S., O. Boucher, N. Bellouin, M. Schulz, Y. Balkanski, J.-L. Dufresne, and M. Pham (2005), Estimates of global multicomponent aerosol optical depth and radiative perturbation in the Laboratoire de Meteorologie Dynamique general circulation model, *J. Geophys. Res.*, *110*, D10S16, doi:10.1029/2004JD004757.
Sato, M., J. Hansen, M. P. McCormick, and J. Pollack (1993), Stratospheric aerosol optical depth, 1850–1990, *J. Geophys. Res.*, *98*, 22,987–22,994.
Savoie, D. L., and J. M. Prospero (1989), Comparison of oceanic and continental sources of non-sea-salt sulphate over the Pacific Ocean, *Nature*, *339*, 685–687.
Sinyuk, A., O. Torres, and O. Dubovik (2003), Combined use of satellite and surface observations to infer the imaginary part of refractive index of Saharan dust, *Geophys. Res. Lett.*, *30*(2), 1081, doi:10.1029/2002GL016189.
Smirnov, A., B. N. Holben, D. Savoie, J. M. Prosepro, Y. J. Kaufman, D. Tanré, T. F. Eck, and I. Slutsker (2000), Relationship between column aerosol optical depth and in situ ground based dust concentrations over Barbados, *Geophys. Res. Lett.*, *27*, 1643–1646.
Smirnov, A., B. N. Holben, T. F. Eck, I. Slutsker, B. Chatenet, and R. T. Pinker (2002a), Diurnal variability of aerosol optical depth observed at AERONET (Aerosol Robotic Network) sites, *Geophys. Res. Lett.*, *29*(23), 2115, doi:10.1029/2002GL016305.

Smirnov, A., B. N. Holben, O. Dubovik, N. T. O'Neill, T. F. Eck, D. L. Westphal, A. K. Goroch, C. Pietras, and I. Slutsker (2002b), Atmospheric aerosol optical properties in the Persian Gulf, *J. Atmos. Sci.*, *59*, 620–634.

Smirnov, A., B. N. Holben, Y. J. Kaufman, O. Dubovik, T. F. Eck, I. Slutsker, C. Pietras, and R. N. Halthore (2002c), Optical properties of atmospheric aerosol in maritime environments, *J. Atmos. Sci.*, *59*, 501–523.

Stenchikov, G. L., I. Kirchner, A. Robock, H.-F. Graf, J. C. Antua, R. G. Grainger, A. Lambert, and L. Thomason (1998), Radiative forcing from the 1991 Mount Pinatubo volcanic eruption, *J. Geophys. Res.*, *103*, 13,837–13,857.

Stenchikov, G. L., K. Hamilton, R. J. Stouffer, A. Robock, V. Ramaswamy, B. Santer, and H.-F. Graf (2006), Arctic Oscillation response to volcanic eruptions in the IPCC AR4 climate models, *J. Geophys. Res.*, *111*, D07107, doi:10.1029/2005JD006286.

Takemura, T., H. Okamoto, Y. Maruyama, A. Numaguti, A. Higurashi, and T. Nakajima (2000), Global three-dimensional simulation of aerosol optical depth distribution of various origins, *J. Geophys. Res.*, *105*, 17,853–17,873.

Takemura, T., T. Nakajima, O. Dubovik, B. N. Holben, and S. Kinne (2002), Single-scattering albedo and radiative forcing of various aerosol species with a global three-dimensional model, *J. Clim.*, *15*, 333–352.

Tanré, D., Y. J. Kaufman, M. Herman, and S. Mattoo (1997), Remote sensing of aerosol over oceans from EOS-MODIS, *J. Geophys. Res.*, *102*, 16,971–16,988.

Tegen, I., and A. A. Lacis (1996), Modeling of particle size distribution and its influence on the radiative properties of mineral dust aerosol, *J. Geophys. Res.*, *101*, 19,237–19,244.

Tie, X., S. Madronich, S. Walters, D. P. Edwards, P. Ginoux, N. Mahowald, R. Zhang, C. Lou, and G. P. Brasseur (2005), Assessment of the global impact of aerosols on tropospheric oxidants, *J. Geophys. Res.*, *110*, D03204, doi:10.1029/2004JD005359.

Toon, O. B., J. B. Pollack, and B. N. Khare (1976), The optical constant of several atmospheric aerosol species: Ammonium sulfate, aluminium oxide, and sodium chloride, *J. Geophys. Res.*, *81*, 5733–5748.

Uchiyama, A., A. Yamazaki, H. Togawa, and J. Asano (2005), Characteristics of Aeolian dust observed by sky-radiometer in the Intensive Observation Period 1 (IPO1), *J. Meteorol. Soc. Jpn.*, *83A*, 291–305.

Volz, F. E. (1973), Infrared optical constants of ammonium sulfate, Sahara dust, volcanic pumice, and flyash, *Appl. Opt.*, *12*, 564–568.

World Climate Program (WCP) (1986), A preliminary cloudless standard atmosphere for radiation computation, World Meteorol. Organ., Geneva, Switzerland.

Wulfmeyer, V., and G. Feingold (2000), On the relationship between relative humidity and particle backscattering coefficient in the marine boundary layer determined with differential absorption lidar, *J. Geophys. Res.*, *105*, 4729–4741.

I. V. Geogdzhayev, NASA GISS, Columbia University, 2880 Broadway, New York, NY 10025, USA. (igor@giss.nasa.gov)

P. Ginoux, L. W. Horowitz, and V. Ramaswamy, NOAA Geophysical Fluid Dynamics Laboratory, Princeton, NJ 08542, USA. (paul.ginoux@noaa.gov; larry.horowitz@noaa.gov; v.ramaswamy@noaa.gov)

B. N. Holben, Biosphere Sciences Branch, NASA Goddard Space Flight Center, Greenbelt, MD 20771, USA. (brent.n.holben@gsfc.nasa.gov)

G. Stenchikov, Department of Environmental Sciences, Rutgers–The State University of New Jersey, 14 College Farm Road, New Brunswick, NJ 08901, USA. (gera@envsci.rutgers.edu)

X. Tie, Atmospheric Chemistry Division, National Center for Atmospheric Research, Boulder, CO 80303, USA. (xxtie@ucar.edu)